HOKKAIDO UNIVERSITY

Title	The effect of liposomal size on the targeted delivery of doxorubicin to Integrin alpha v beta 3-expressing tumor endothelial cells
Author(s)	Kibria, Golam; Hatakeyama, Hiroto; Ohga, Noritaka et al.
Citation	Biomaterials, 34(22), 5617-5627 https://doi.org/10.1016/j.biomaterials.2013.03.094
Issue Date	2013-07
Doc URL	https://hdl.handle.net/2115/53030
Type	journal article
File Information	01 Title page.pdf

Hokkaido University Collection of Scholarly and Academic Papers : HUSCAP

The effect of liposomal size on the targeted delivery of doxorubicin to Integrin αvβ3-expressing tumor endothelial cells

Golam Kibria[1], Hiroto Hatakeyama[1], Noritaka Ohga[2], Kyoko Hida[2], Hideyoshi Harashima[1*]

[1]Laboratory of Innovative Nanomedicine, Faculty of Pharmaceutical Sciences, Hokkaido University, Kita 12, Nishi 6, Kita-ku, Sapporo 060-0812, Japan
[2]Division of Vascular Biology, Graduate School of Dental Medicine, Hokkaido University, Kita 13 Nishi 7, Kita-ku, Sapporo 060-8586, Japan

*Corresponding author

Hideyoshi Harashima
Professor
Faculty of Pharmaceutical Sciences
Hokkaido University
Sapporo, Hokkaido, 060-0812, Japan.
Tel.: +81 11 706 3919, Fax: +81 11 706 4879.
E-mail: harasima@pharm.hokudai.ac.jp

Running Headline: Size controlled liposome for tumor vasculature targeting

Abstract

Size of the liposomes (LPs) specially governs its biodistribution. In this study, LPs were developed with controlled sizes, where variation in LP size dictates the ligand-receptor interaction, cellular internalization and its distribution within the tumor microenvironment. The therapeutic efficacies of doxorubicin (DOX)-loaded RGD modified small size (~100 nm in diameter, dnm) and large size (~300 dnm) PEGylated LPs (RGD-PEG-LPs) were compared to that of Doxil (a clinically used DOX-loaded PEG-LP, ~100 dnm) in DOX resistant OSRC-2 (Renal cell carcinoma, RCC) tumor xenografts. Doxil, which accumulated in tumor tissue via the Enhanced Permeability and Retention (EPR) effect, failed to suppress tumor growth. Small size RGD-PEG-LP, that targets the tumor endothelial cells (TECs) and extravasates to tumor cells, failed to provide anti-tumor effect. Large size RGD-PEG-LP preferentially targets the TECs via minimization of the EPR effect, and significantly reduced the tumor growth, which was exerted through its strong anti-angiogenic activity on the tumor vasculature rather than having a direct effect on DOX resistant RCC. The prepared large size RGD-PEG-LP that targets the TECs via interacting with Integrin $\alpha v\beta 3$, is a potentially effective and alternate therapeutic strategy for the treatment of DOX resistant tumor cells by utilizing DOX, in cases where Doxil is ineffective.

1. Introduction

Liposomes (LPs) have been extensively studied as drug delivery systems. The size of a LP is a major determinant of its biodistribution as well as the systemic stability. Small size PEGylated LPs (PEG-LPs) of around 100 nm in diameter (dnm) are widely used to target many diseased tissues including cancer [1-4]. Doxil, a typical successful example of doxorubicin (DOX) loaded small size PEGylated liposome (PEG-LP) (~100 dnm), functions against the tumor cells via the enhanced permeability and retention (EPR) effect [3, 4]; and when modified with specific ligands, has been used previously to target the tumor vasculature [5-7]. In previous studies, the interaction of PEG-LP modified with CD13 with NGR was used to target the vasculature of GI-LI-N, HTLA-230 and IMR-32 neuroblastoma tumors [5], where the IC50 values for these cells to DOX were found to be 0.4 μM, 0.6 μM and 0.02 μM, respectively [8, 9]. Later, the recognition of Integrin αvβ3 by RGD modified PEG-LP was used to target the vasculature of an SN12C renal cell carcinoma (RCC) [6]; where the EC50 value of the SN12C cells to DOX was found to be 50 ng/ml [10]. Additionally, NG2 Proteoglycan interacting TAASGVRSMH/LTLRWVGLMS [11], a membrane type-1 matrix metalloproteinase (MT1-MMP) interacting GPLPLR [12] and the APRPG ligand (the target receptor is unknown at present) [13] modified PEG-LPs were used to target the vasculatures of melanoma (B16F10), Colon 26 NL-17 and glioblastoma tumors, respectively. It should be noted that the compatibility of the selected target molecules and the specific ligand is an important issue in terms of exerting the pharmacological effect of the nanoparticles against a tumor type.

The endothelial cell gaps in the tumor vasculature are much higher (~100-600 nm) [14] than that of the normal endothelium (<6 nm) [15]; therefore, it is much

easier for small size PEG-LPs (60-150 dnm) to extravasate to tumor cells [2, 4], a process called the EPR effect. On the other hand, large size particles (>200 dnm) more promptly adhere to the target cells by facilitating ligand-receptor interactions [16-18], despite their limitations related to their recognition by reticuloendothelial system (RES) as well as being entrapped in splenic sinusoidal filters [19-21]. Therefore, we hypothesized that large size PEG-LP would be more effective in terms of targeting diseased tissues once they were modified with a specific ligand. In this study, we prepared small size (~100 dnm) and large size (~300 dnm) PEG-LPs modified with RGD ligand (RGD-PEG-LPs). The effect of the size of PEG-LPs on cellular internalization, ligand-receptor interactions as well as on in vitro drug delivery efficiency was evaluated using human umbilical vein endothelial cells (HUVEC) that express Integrin αvβ3 [22]. To observe the tissue distribution as well as the therapeutic effect, size controlled PEG-LPs were applied to mice bearing kidney cancer (human RCC), which is notoriously resistant to chemotherapy [23-27], where various multidrug-resistant proteins are responsible for drug resistance. Because of this, it would be difficult to treat RCC by delivering a drug to tumor cells. In tumor tissue, vascular endothelial cells (TECs) play a critical role in tumor growth and progression by providing nutrients, oxygen, growth factors etc. to tumor cells [7, 28, 29]. The frequent mutation of the von Hippel-Lindau (VHL) protein triggers the up-regulation of vascular endothelial growth factor (VEGF) production and results in the progression of highly angiogenic RCC tumors [30]. Sunitinib, Sorafenib and Bevacizumab have been approved for the treatment of RCC which function against VEGF and VEGF receptors (VEGFRs) [31, 32], suggesting the effectiveness of anti-angiogenic therapy against RCC. However, RCC can become resistant to these drugs [33-35], which also have a number of side effects, including cardiac toxicity, hepatotoxicity,

hypothyroidism, anemia, hand-foot syndrome etc. [36]. Therefore, as an alternate approach, a drug delivery system that targets the tumor vasculature would be necessary for RCC tumor therapy.

For targeting the vasculature in OSRC-2 (RCC) tumor tissue, we recently developed a large size PEG-LP (~300 dnm) modified with two different types of ligands ((CD13 specific ligand NGR; and a non-specific cell penetrating peptide, tetra-arginine (R4)) which exhibited better anti-tumor effect, as NGR alone showed poor therapeutic efficacy [37]. While the NGR motif exerts its efficiency in other tumor types [5], its activity with respect to RCC is poor. The findings of the present study indicate that large size PEG-LP, modified only with a single ligand RGD (RGD-PEG-LP) which interacts with Integrin αvβ3, is efficient to both targeting and disrupting the tumor vasculature in OSRC-2 tumor tissue. Additionally, we provide more evidences and a mathematical explanation for the therapeutic efficacy of large size RGD-PEG-LP over the small size versions against the RCC tumor model.

To overcome the limitations associated with the drug resistance of RCC as well as considering the side effects of on-going therapy; we proposed an active targeting liposomal delivery system aimed at treating RCC by delivering DOX to TECs via targeting the Integrin αvβ3 receptor. We prepared DOX loaded small size (~100 dnm) and large size (~300 dnm) RGD-PEG-LPs and their anti-tumor activity was investigated and compared with Doxil in mice bearing human RCC (OSRC-2) tumors.

2. Materials and Methods

2.1. Materials

Hydrogenated soybean phosphatidylcholine (HSPC), Egg phosphatidylcholine (EPC), Cholesterol, N-(lissamine rhodamine B sulfonyl)-1,2-dioleoyl-sn-glycero-3-phosphoethanolamine (rhodamine-DOPE), 1,2-distearoyl-sn-glycero-3-phosphoethanolamine-N-[methoxy(polyethyleneglycol)-2000] (PEG-DSPE) were purchased from Avanti Polar Lipids (Alabaster, AL, USA). cRGDfK peptide was purchased from Peptides International, Inc. (Louisville, KY, USA) and conjugated with PEG-DSPE as reported before [22]. Doxorubicin Hydrochloride was purchased from Wako Pure Chemical Industries (Osaka, Japan). ^{3}H-Cholesterylhexadecyl ether (^{3}H-CHE) was purchased from PerkinElmer Life Science (MA, USA). RPMI 1640 were purchased from Sigma (St. Louis, MO, USA). EGM-2 and EGM-2 MV medium were purchased from Lonza (Walkersville, MD, USA).

2.2. Isolation of mouse tumor endothelial cells (TECs)

OSRC-2 tumor endothelial cells (OSRC-EC) were isolated as described previously [38-40]. Briefly, TECs were isolated from OSRC-2 tumors and dermal tissue in tumor-bearing mice using a magnetic cell sorting system (MACS; Milteny Biotec). TECs were plated onto 1.5% gelatin-coated culture plates and grown in EGM-2MV (Clonetics) and 15% fetal bovine serum (FBS). Diphtheria toxin (500 ng/ml; Calbiochem) was added to TEC subcultures to kill any remaining human tumor cells.

2.3. Cell lines and culture

Human renal cell carcinoma (RCC), OSRC-2 cells (Riken Cell Bank, Tsukuba,

Japan) were cultured in RPMI 1640 supplemented with heat-inactivated 10% FBS and penicillin (100 units/ml), streptomycin (100 μg/ml) under an atmosphere of 5% CO_2 at 37 °C, and used within 6 months of purchasing. OSRC-EC and Human umbilical vein endothelial cells (HUVEC) were cultured in EGM-2 MV and EGM-2 medium, respectively.

2.4. Animal experiments

BALB/cAJcl-nu/nu male mice (CLEA, Japan), 4 weeks of age were allowed to food and water under controlled environmental conditions. Animal experiments were performed according to the national regulations and approved by the Hokkaido University Animal Care Committee.

2.5. Preparation of PEG-LPs

2.5.1. Preparation of PEG-LPs for in vitro cellular uptake

LPs composed of EPC and Cholesterol (molar ratio: 7/3) were prepared by the lipid film hydration method. After evaporation under nitrogen gas, dried lipid films were hydrated with phosphate buffer saline (PBS, pH 7.4), followed by vortexing. During film formation, 1.5 mol% rhodamine-DOPE was incorporated to label the lipid composition. To prepare large size particles, the prepared LPs were extruded through a 0.4 μm polycarbonate filter. To prepare small size particles, the dried lipid films were hydrated with PBS (pH 7.4) followed by sonication in a bath-type sonicator (AU-25C, Aiwa, Japan). The prepared LPs were extruded through a 0.08 μm polycarbonate filter to control the size. After extrusion, the total lipid concentration in LPs was determined. LPs were incubated with 5 mol% PEG-DSPE or RGD-PEG-DSPE at 60 °C for 30 min to prepare PEG-LP or RGD-PEG-LP, respectively.

2.5.2. Preparation of PEG-LPs for biodistribution study

Large size as well as small size PEG-LPs composed of EPC and Cholesterol (molar ratio: 7/3) were prepared by following the same process as described above. During film formation, ^{3}H-CHE was added as a nonexchangeable, nonmetabolizable lipid phase marker.

2.5.3. Preparation of PEG-LPs for tumor accumulation study

Large size as well as small size PEG-LPs composed of EPC and Cholesterol (molar ratio: 7/3) were prepared by following the same process as described above. During film formation, 1 mol% rhodamine-DOPE was incorporated to label the lipid composition.

2.5.4. Preparation of DOX loaded PEG-LPs

LPs composed of HSPC:Cholesterol (7:3) were prepared by lipid film hydration method followed by extrusion to control the size. DOX was loaded to the LPs by following the ammonium sulfate gradient method [41, 42]. Five mol% PEG or RGD-PEG was added to prepare PEG-LPs (DOX) or RGD-PEG-LPs (DOX), respectively (details are given in supplementary data).

2.6. Characterization of PEG-LPs

The mean size and zeta potential of the prepared PEG-LPs were determined using a Zetasizer Nano ZS ZEN3600 instrument (Malvern Instruments Ltd., Worchestershire, UK).

2.7. Cellular uptake of small and large size PEG-LPs

To investigate the cellular uptake of the different size PEG-LPs, 100000 HUVEC

cells were seeded on a 35-mm glass-bottom dish (Iwaki, Chiba, Japan) in 2 ml of culture medium for 24 h. The next day, the cells were washed with PBS and incubated with PEG-LPs (100 nmol lipid/2ml) in Kreb's buffer for 2 h at 37 °C. After 1.5 h of incubation, 5 μl of Hoechst 33342 (1 mg/ml) (Dojindo) was added to stain the nuclei and the suspension was reincubated for an additional 30 min. The medium was then removed followed by washing with PBS. Finally, 1 ml of Krebs buffer was added and the cells were observed by confocal laser scanning microscopy, CLSM (Nikon A1, Nikon Instruments Inc., Tokyo, Japan). The total number of pixel of internalized PEG-LPs in each confocal image was calculated by using ImagePro-plus software (Media Cybernetics Inc., Bethesda, MD, USA).

2.8. Evaluation of binding constant

To determine the binding constant (Kd value), the cellular uptake of the prepared RGD-PEG-LPs was measured. HUVEC (40000 cells/well) were seeded on 24-well plates. The next day, the cells were incubated with 500 μl of media consisting 5, 10, 50, 100, 150, 200 μl of LP and remaining part of the Kreb's buffer for 2 h at 37 °C. Finally, the cell supernatant was collected by centrifugation at 12000 rpm, 4 °C for 5 min and fluorescence intensity was measured (550nm-590nm). Number of particles was calculated based on the size and lipid dose of the RGD-PEG-LPs [43-45]. Sigma-plot 12.0 (Systat Software, San Jose, CA, USA) was used to calculate the binding constant (Kd) and maximum binding (Bmax) values for small and large size RGD-PEG-LPs.

2.9. Inhibition of cellular uptake of the RGD-PEG-LPs by free RGD

To examine the effect of excess amount of free peptides on the cellular uptake of different size RGD-PEG-LPs, a cellular uptake experiment was performed in the

presence of different concentration of free RGD peptide. HUVEC cells were seeded on a 35-mm glass-bottom dish. Excess RGD peptide (fold v.s. RGD peptide present on the surface of RGD-PEG-LPs used) in Kreb's buffer were added to the prepared glass bottom dish and incubated for 5 min at 37 °C in an atmosphere of 5% CO_2 and 95% humidity. After 5 min, RGD-PEG-LPs were added and incubated for next 20 min at 37 °C. The cells were washed 3 times with phosphate buffered saline (PBS). Finally, Kreb's buffer was added to each dish followed by CLSM observations.

2.10. Biodistribution of PEG-LPs in tumor-bearing mice

OSRC-2 cells were inoculated on the back of BALB/c nude mice. At a tumor volume of 200-250 mm^3, mice were injected by tail vein with ^{3}H-CHE-labeled PEG-LPs (0.5 μmol lipid/200 μl). At 24 h after injection, blood and other organs were collected and radioactivity was measured (details are given in supplementary data).

2.11. In vivo targeting of PEG-LPs to tumor vasculature

At a tumor volume of 100 mm^3, mice bearing OSRC-2 tumor were injected with rhodamine-labeled PEG-LPs (0.5 μmol lipid/200 μl). At 6 h after injection, animals were anesthetized and tumors were collected, followed by immunostaining with FITC-conjugated griffonia simplicifolia isolectin B4 (GS-IB4-FITC) (Vector Laboratories Inc.) for TECs and with Hoechest 33342 for nuclei followed by CLSM analysis.

2.12. In vivo anti-tumor efficacy

DOX loaded PEG-LPs were injected to OSRC-2 tumor (~150 mm^3) bearing mice

(n=4-5) with once daily dose of 1.5 mg DOX/kg body weight or with PBS (control) for the first three days (total of 3 injections). Body weights and tumor volumes were recorded at three day intervals. Tumor volume was calculated using the formula: $1/2 \times a \times b^2$, where a and b represent the largest and smallest diameters of tumors, respectively. A slope of tumor volume-time curve, representing the growth rate, of each tumor in the treatment group (T) was calculated and divided by that in the control group (C) to give an index (T/C) for the in vivo therapeutic effect, as reported before [46].

2.13. Detection of cell apoptosis

Mice bearing OSRC-2 tumor (~100 mm^3) were injected with once daily dose of 1.5 mg DOX/kg body weight (n=3) for the first three days. At day 4, 200 μl of Apo-Trace solution (Sigma-Aldrich Inc.) was injected via tail vein and incubated for 1.5 h. Mice were anesthetized, tumors and other organs were collected followed by incubation with Alexa Fluor 647-Isolectin (GS-IB4) solution (Invitrogen) to stain the blood vessels followed by CLSM analysis. The total number of pixels of apoptotic cells (green) in each confocal image of the collected organs was calculated by using ImagePro-plus software.

2.14. Anti-angiogenic effect of PEG-LPs (DOX)

Similar dosing of DOX as above was followed for the first three days. At day 4, animals were anesthetized, tumors and other organs were collected, followed by immunostaining with FITC-isolectin for blood vessels and with Hoechest 33342 for nuclei. Anti-angiogenic effect of PEG-LPs was observed under CLSM. The total number of pixel of blood vessel (green) as well as of cell nuclei (blue) in each confocal image of the collected organs were calculated by using ImagePro-plus

software.

2.15. Cytotoxicity assay

The sensitivity of OSRC-2 (RCC) and OSRC-EC (TEC) cells to DOX was determined by the in vitro WST [2-(2-methoxy-4-nitrophenyl)-3-(4-nitrophenyl)-5-(2,4-disulfophenyl)-2H-tetrazolium, monosodium salt] assay protocol. Briefly, 5,000 cells were plated in 96-well plates and incubated overnight. The next day, the cells were exposed to different concentrations of free DOX at 37 °C for 8 h, followed by reincubation for 16 h in the presence of fresh media. The cells were washed with PBS and re-incubated with cell counting kit-8 (CCK-8) solution (Dojindo) for 2 h and absorbance was measured at 450 nm using a microplate reader (Thermo Fisher Scientific Inc.). To measure DOX uptake, 40,000 cells were seeded in 24-well plates and allowed to stand overnight. The next day, the cells were exposed to free DOX (10 μg/ml) at 37 °C for 8 h, followed by washing with PBS. The cell supernatant was collected by centrifuging at 12000 rpm, 4 °C for 5 min and fluorescence intensity was measured (450nm-590nm).

2.16. Toxicological study

Mice bearing OSRC-2 tumor (~100 mm^3) were injected with once daily dose of 1.5 mg DOX/kg body weight (n=3) for the first three days. At day 4, animals were anesthetized and blood samples were drawn and allowed to stand at 4 °C for coagulation. Serum was collected by centrifuging the coagulated blood at 10,000 rpm at 4 °C for 10 min. Serum alanine transaminase (ALT) and aspartate amino transferase (AST) enzyme levels were determined using a commercially available kit (Wako) by following the manufacturer's instructions.

2.17. Statistical analysis

Comparisons between multiple treatments were made using the one-way analysis of variance (ANOVA), followed by the Dunnett test. Pair-wise comparisons of subgroups were made using the student's t-test. Differences among means were considered to be statistically significant at a p value of <0.01 and <0.05.

3. Results

3.1. Characterization of LPs

Liposomes composed of EPC (or HSPC) and cholesterol (7:3) were prepared by the lipid film hydration method followed by extrusion to control the size. The average diameter of small and large size PEG-LPs were determined to be ~120 nm and ~330 nm respectively, with a narrow size distribution and comparable surface charge (Fig. 1A, Table 1). The encapsulation efficiencies of DOX in the small size PEG-LP, the small size RGD-PEG-LP and the large size RGD-PEG-LP were determined to be 98%, 97% and 96% respectively. Similar physical properties as above were found for DOX loaded PEG-LPs (Table S1).

3.2. Size dependent binding of RGD-PEG-LPs to endothelial cells

To observe the effect of size on the cellular association of PEG-LPs, in vitro cellular uptake was measured at 37 ^{0}C in HUVEC which express remarkable levels of Integrin αvβ3 [22]. Based on qualitative and quantitative analyses, the signals detected from small and large size PEG-LP (Fig. 1B-C) were negligible, indicating that only an increase in the size of PEG-LP does not result in an enhancement in cellular uptake. On the other hand, the small size RGD-PEG-LP showed a greater extent of cellular uptake and a further enhancement was observed for the large size RGD-PEG-LP (Fig. 1B-C).

Based on these results, we next quantitatively determined the binding constant (Kd) for the small and large size RGD-PEG-LPs at 4 °C and 37 °C in HUVEC. Compared to small size, large size RGD-PEG-LP showed about a 10 times higher rate of binding and cellular uptake efficiency (Fig. 1D, Table 1). This was also tested by determining the inhibition of cellular uptake of RGD-PEG-LPs using

free RGD (Fig. 1E). Compared to large size, the cellular uptake of small size RGD-PEG-LP was more rapidly inhibited by free RGD; indicating that, compared to small size, large size RGD-PEG-LP caused higher multivalent interactions with Integrin αvβ3 which facilitates its prompt internalization (Fig. 1F). These results suggest that large size particles might have the preference to target the diseased tissues.

3.3. Distribution of PEG-LPs in tumor tissues

Based on the above results, we next applied the PEG-LPs to mice bearing OSRC-2 (RCC) tumor. To examine the localization of PEG-LPs within the tumor tissue, mice were injected with [^{3}H]CHE labeled PEG-LPs. Higher amounts of small size PEG-LP were found in the tumor via the EPR effect due to its long circulation property mediated by PEGylation (Fig. 2A). However, the tumor accumulation of large size PEG-LP was lower, which can be attributed to the entrapment of the particles in the splenic filter (Fig. S1A) and possibly from escaping the EPR effect, as indicated by the size dependent distribution of PEG-LPs (Fig. S1B). On the contrary, a similar pattern of accumulation of both small and large size RGD-PEG-LPs was observed in tumors (Fig. 2A) and other tissues (Fig. S1A), indicating its ligand dependent distribution (Fig. S1B). Compared to large size PEG-LP, the tumor accumulation of large size RGD-PEG-LP was found to be higher (Fig. 2A), suggesting that it likely targets the tumor vasculature.

3.4. Association of PEG-LPs to tumor vasculature

Tumor vasculature targeting efficiency was investigated by injecting mice with rhodamine labeled-PEG-LPs. Based on CLSM analyses, a huge amount of small size PEG-LP was found throughout the tumors, indicating that it extravasated

and accumulated in the tumor via the EPR effect (Fig. 2B, Fig. S2). However, only a very small amount of large size PEG-LPs was detected in the tumor, which can be attributed to its lower rate of extravasation through the tumor vasculature. On the other hand, the accumulation of small size RGD-PEG-LP in tumors was found to be minimal, due to its lower systemic stability as well as its recognition by the spleen (Fig. S1A). However, a larger amount of large size RGD-PEG-LP was detected in tumors where most of the signals had merged and were located within the tumor blood vessels (Fig. 2B, Fig. S2), indicating its higher tumor vasculature targeting efficiency. These results clearly indicate that the large size PEG-LP could minimize the EPR effect and preferentially target the TECs, provided it is modified with the specific ligand RGD.

3.5. Drug-resistant tumor therapy by DOX loaded PEG-LPs

The therapeutic application of the large size particles was observed and compared to that of the small size particles. Mice bearing OSRC-2 tumor were intravenously injected with 1.5 mg DOX in PEG-LPs/kg body weight. Tumor volumes and life span of mice are presented in Fig. 3. Compared to controls, Doxil was essentially ineffective in inhibiting tumor growth (Fig. 3A). Furthermore, small size RGD-PEG-LP (DOX) failed to show an anti-tumor effect. On the other hand, large size RGD-PEG-LP (DOX) surprisingly exerted a significant anti-tumor effect (Fig. 4A) and prolonged the life span of the mice (Fig. 3B). The index for in vivo therapeutic effect (T/C) was calculated to compare the efficacy of the PEG-LPs (DOX) (Table S2). The lower T/C value for large RGD-PEG-LP (DOX) clearly indicates its anti-tumor efficacy as compared to the others.

3.6. Mechanism of the anti-tumor effect

To elucidate the mechanism responsible for the therapeutic action of the PEG-LPs (DOX), the induction of apoptosis within tumors was evaluated (Fig. 4). Compared to controls, almost no apoptotic cells were detected in tumors that had been treated with Doxil (Fig. 4A-B). This result is indicative of the general tendency for RCCs to be resistant to DOX in an in vivo situation, which leads to the failure of Doxil to exert an anti-tumor effect. In contrast, a greater amount of apoptotic cells was detected throughout the tumors treated with both small and large size RGD-PEG-LPs (DOX) (Fig. 4A-B); where in tumors treated with small size RGD-PEG-LP (DOX), apoptotic cells were also found both inside and outside the tumor vessels (Fig. 4A), indicating that it can target TECs and can enter tumor cells as well via the EPR effect. However, in the case of large size RGD-PEG-LP (DOX)-treated tumors, most of the apoptotic cells were detected surrounding the tumor vessels (Fig. 4A) where it merged and a greater extent of apoptotic endothelial cells was found, as compared to its small size version (Fig. 4C); indicating that large size RGD-PEG-LP (DOX) largely targets and kills the TECs.

Further, the structure of tumor vessels was observed after injecting the mice with PEG-LPs (DOX). A tumor vessel network was clearly observed in the Doxil treated tumors, similar to the controls (Fig. 4D), indicating that Doxil has no effect on the area of tumor vessels (Fig. 4E) and associated nuclei (Fig. 4F). Small size RGD-PEG-LP (DOX) partially dismantled (Fig. 4D) and reduced the area (Fig. 4E) of tumor vessels, indicating its efficiency for targeting the tumor vasculature, however, no effect on the area of the nuclei was detected (Fig. 4F), indicating that this activity was not sufficient to kill the tumor cells themselves. On the other hand, tumor vessels were clearly destroyed and disappeared in the case of tumors that had been treated with large size RGD-PEG-LP (DOX) (Fig. 4D), and the area

of the tumor vessels was significantly reduced (Fig. 4E), indicating that it efficiently targeted the tumor vasculature where it remained attached or internalized into the TECs (Fig. 2B). This is consistent with the significant reduction in the area of nuclei (Fig. 4F) as the result of the passive killing of tumor cells. These results indicate that a lower dose of DOX in large size RGD-PEG-LP is efficient to target and kill TECs as well as to disrupt the tumor vasculature.

3.7. Comparison of the sensitivity of tumor cells and tumor endothelial cells to DOX

To support the remarkable apoptotic effect of large size RGD-PEG-LP (DOX) on the TECs in vivo condition, we have evaluated the sensitivity of tumor cells and TECs to DOX. OSRC-ECs were isolated from OSRC-2 tumors as described previously [38-40]. OSRC-2 and OSRC-EC were exposed to different concentrations of free DOX and the sensitivity to DOX was compared. The results showed that OSRC-EC appears to be about 100 times more sensitive to DOX (as evidenced by a 50% reduction in cell viability) compared to OSRC-2 (Fig. 5A), indicating the resistance of OSRC-2 tumor cells to DOX. Even though, at a dose of 10 μg DOX/ml, the amount of DOX in OSRC-2 was found to be 1.5 times higher than that of OSRC-EC (Fig 5B), OSRC-2 resulted in nearly complete survival. These studies clearly demonstrate that delivering DOX to TECs (OSRC-EC) holds some promise for treating DOX resistant OSRC-2.

3.8. Effect of PEG-LPs (DOX) on normal organs

To observe the effect of DOX loaded PEG-LPs on normal organs, we first evaluated the morphology of blood vessels of the liver, spleen and lung of the

OSRC-2 tumor bearing mice. Based on the CLSM analysis, no unusual changes in the blood vessel structures were observed (Fig. 6A). Additionally, as markers for hepatotoxicity, the serum ALT and AST enzyme levels of OSRC-2 mice treated with PEG-LPs (DOX) were also measured (Fig. 6B-C) and no significant difference in these enzymes levels was observed among the treated groups.

4. Discussion

Small size PEG-LPs having ~100 dnm are generally used to target the tumor tissues via the EPR effect [2-4]. We recently reported that the size of LPs has impact on the EPR effect as well as on the targetability of the nanoparticles [37]. In this study, we evaluated the ligand-receptor interaction, drug delivery efficiency and the mechanism of the therapeutic effect as a function of the size of PEG-LPs. The cellular uptake was performed using small size (~100 dnm) and large size (~300 dnm) RGD-PEG-LPs in HUVEC (Fig. 1). Compared to small size, large size RGD-PEG-LP exhibited about a 10 times higher multivalent binding towards its target receptor (Table 1), facilitating the enhancement in cellular association, even though the Bmax values were found to be consistent and temperature dependent. Additionally, the number of RGD molecules present on the surface of one large size RGD-PEG-LP was estimated to be ~12.5 times higher than that of the small size version. Therefore, the more rapid cellular internalization of large size RGD-PEG-LP (Fig. 1B) can be attributed to the stronger multivalent binding of the RGD motif to its receptor [47], which finally leads to a higher amount of DOX being delivered to target cells (Fig. S3). These results indicated that large size particles have better preference to target the diseased tissues.

We, next evaluated the distribution of PEG-LPs in tumor tissue. In an in vivo situation, the distribution of PEG-LPs in tumor bearing mice was found to be size dependent, where as RGD-PEG-LPs directed a ligand dependent distribution (Fig. 2, Fig. S1). Based on the confocal microscopic analysis, a huge amount of small size PEG-LP was detected in the tumor tissue where it accumulates through the extravasation of the leaky vasculature of RCC tumors (Fig. 2B), a process known

as the EPR effect. On the other hand, the accumulation of large size PEG-LP in tumor tissue was found to be negligible (Fig. 2B), indicating that the particles having a ~300 dnm could not provide the EPR effect. Therefore, minimization of extravasation might lead to larger number of large size PEG-LP to remain in the tumor vasculature once it is modified with RGD (RGD-PEG-LP) that finally facilitates the multivalent binding towards its receptor (Fig. 2B), which is present on the surface of TECs (Fig. 1F). In the case of tumor tissue, the small size RGD-PEG-LPs were found to be located both inside and outside the tumor vasculature (Fig. 2B), where most of the signals of the large size RGD-PEG-LPs were detected along with the tumor vasculature. These results indicate that controlling the size of PEG-LPs governs not only its distribution but also dictates the site-specific delivery within the tumor microenvironment.

Based on the above results, it indicated that RGD ligands present on the surface of large size particles have promising advantages to target the TECs of tumor tissue. Therefore, the therapeutic effect of RGD-PEG-LPs (DOX) was observed and compared with that of Doxil in mice bearing RCC tumors. Doxil itself failed to inhibit tumor growth (Fig. 3A), as it accumulated in OSRC-2 tumor cells which are resistant to DOX (Fig. 5A). Unexpectedly, small size RGD-PEG-LP (DOX) had no effect against tumor growth. Conversely, large size RGD-PEG-LP with a lower dose of DOX resulted in a significant reduction in tumor growth (Fig. 3A), despite the similar biodistribution to its small size version (Fig. S1B). These results raised the question as to the reason for the better therapeutic effect of large size RGD-PEG-LP over its small size version.

To explore the mechanism of the size dependent therapeutic effect of PEG-LPs (DOX), we next evaluated the induction of apoptosis in tumor tissues. Doxil failed to induce apoptosis in tumor tissues (Fig. 4A-B). In contrast, a huge amount of apoptotic cells was detected in tumors that had been treated with both small and large size RGD-PEG-LP (DOX) (Fig. 4A), however no significant difference in the area of the apoptotic cells was observed between these two groups (Fig. 4B). We further calculated the % of apoptotic cells that were co-localized with tumor vessels (Fig. 4C). The extent of co-localization of apoptotic cells with tumor vessels (Fig. 4C), as indicated by arrows (Fig. 4A), was significantly higher in tumors that had been treated with large size RGD-PEG-LP (DOX), but not for the small size version, where such co-localizations were rarely observed. These results indicate that large size RGD-PEG-LP (DOX) preferentially targets and kills the TECs, where the small size largely acts directly on tumor cells.

Furthermore, the effect of PEG-LPs (DOX) on the morphology of tumor vessels was evaluated. Both the small and large size RGD-PEG-LP (DOX) clearly destroyed the tumor vessels (Fig. 4D), as indicated by the area of the vessels (Fig. 4E), where the large size version had a stronger effect. However, only the large size RGD-PEG-LP (DOX) significantly reduced the number of nuclei (Fig. 4F), indicating the death of tumor cells in a blood supply-dependent manner. These results revealed that large size RGD-PEG-LP was able to readily approach tumor vessels, and to efficiently bind to them, which would result in efficient internalization; consequently, to deliver higher amounts of DOX to the TECs where it provides a superior cytotoxic effect, since the large size LP (~300 dnm) possesses about a 10 times higher internal volume than the small size (~100 dnm) [43]. After disruption of the tumor vasculature, the blood supply within the tumor

microenvironment would be discontinued resulting in the eventual death of the tumor cells. To investigate the cytotoxic effect of large size RGD-PEG-LP (DOX) on the TECs in tumor vasculature, we additionally compared the sensitivity of RCC tumor cells (OSRC-2) and TECs (OSRC-ECs) isolated from RCC tumor tissue to DOX; where, the OSRC-ECs show higher sensitivity to DOX, as compared to OSRC-2 cells (Fig. 5A). Generally, tumor cells grow at a faster rate than other cells including TECs, which might affect cell viability (Fig. 5). To assess this issue, we evaluated the growth rate of OSRC-2 and OSRC-ECs over 24 h; however, no significant difference in growth rates of the cells was observed (Fig. S4). Therefore, the effect of growth rate on cell viability can be excluded. These findings indicate the sensitivity of OSRC-ECs to DOX, suggesting that TECs are a promising target for the delivery of DOX in treating RCC. Therefore, the in vivo anti-tumor effect of large size RGD-PEG-LP in OSRC-2 tumor-bearing mice can be attributed to the specific apoptotic effect on TECs followed by rapid destruction of tumor vasculatures, known as anti-angiogenic effect, rather than on OSRC-2 tumor cells (Fig. S5). This result is supported by the previous reports showing that anti-angiogenic therapy would be effective in suppressing the growth of RCC tumors [31, 32].

The RGD motif is readily recognized by Integrin αvβ3 that is expressed largely by TECs [6, 7] as well as more limitedly from normal endothelial cells of the spleen, lungs etc. [48, 49]. Therefore, it is necessary to evaluate the effect of RGD-PEG-LPs (DOX) on normal organs. We first evaluated the morphology of blood vessels of the major organs. No remarkable changes in the blood vessel structures were observed (Fig. 6A). Additionally, the induction of apoptosis by PEG-LPs (DOX) in normal organs was evaluated (Fig. S6). Although the

preparations exhibited a size dependent induction of apoptosis in normal organs; however, the magnitude of the effects was only about 2-fold as compared to the control. Additionally, as the liver is the major clearance organ for nanoparticles, the serum ALT and AST enzyme levels of OSRC-2 mice were also measured (Fig. 6B-C). Although large size RGD-PEG-LP (DOX) showed a 20% reduction in liver blood vessel area (Fig. S7), no significant difference in above enzymes levels was observed among the treated groups (Fig. 6B-C). Additionally, our system shows anti-tumor effect at lower dose of DOX as compared to others where a higher doses of DOX was used [50-52]. Therefore, due to lower dose of DOX, large size particle would not provide any serious toxicity in liver and spleen despite its higher accumulations (Fig. S1). Moreover, no significant difference in body weights of the treated mice and the control group was observed (data not shown). Collectively, these results indicate that the preparations might not appear to have any serious toxicity.

Based on the results obtained in the present study, we propose the following mechanism for the anti-tumor effect of large size RGD-PEG-LP (DOX). In an in vitro study, 40000 OSRC-2 cells were incubated with a dose of 10 μg/ml DOX and the amount of internalized DOX was determined to be 23.7×10^{-4} ng/cell, which caused the death of about 20% of the cells (Fig. 5A). On the other hand, OSRC-2 tumor bearing mice (20 g body weights) were injected with 3 μg of DOX (1.5 mg/kg) and the amount of Doxil in tumors via the EPR effect was found to be 3 %ID/g tumor (Fig. 2A), where 1 g of tumor tissue contains 10^8 cells [53]. Hence, the availability of DOX would be 90×10^{-8} ng/tumor cell (Fig. 7), which is about 2600 times lower than the dose found in the in vitro situation, indicating that, to kill 20% of the tumor cells in an RCC tumor, a ~2600 times higher amount of Doxil

would be required, which is a practical impossibility. Therefore, an insufficient amount of DOX in tumor cells delivered by Doxil fails to provide a sufficient anti-tumor effect. On the other hand, TECs (OSRC-EC) derived from OSRC-2 tumor tissue were found to be ~100-fold more sensitive to DOX than OSRC-2 cells (Fig. 5A). At a dose of 10 μg/ml DOX to OSRC-EC, the internalized DOX/cell was found to be 2.38×10^{-4} ng, which causes the death of about 80% of cells (Fig. 5A). In addition, at a dose of 3 μg DOX/20g body weight of mice, the amount of large size RGD-PEG-LP (DOX) was found to be 2.5 %ID/g tumor (Fig. 2A), where most of the particles targeted the TECs (Fig. 2B). TECs represent about 2% of tumor tissue (2×10^6 cells/g tumor) [38, 54], the availability of DOX in one TEC would be 37.5×10^{-6} ng (Fig. 7), which is only 6 times lower than the DOX found in vitro conditions. It is feasible that a ~6 times higher amount of DOX delivered by the large size RGD-PEG-LP (DOX) would be able to kill ~80% of the OSRC-ECs in OSRC-2 tumors. Furthermore, the number of tumor cells is about 100-times greater than the TECs in tumor tissues [38, 54, 55], hence attacking one TEC would lead the suppression of growth or death of many surrounding tumor cells [29, 56]. Compared to the DOX delivered by Doxil to tumor cells, about 40 times higher amount of DOX could be delivered by large size RGD-PEG-LP to TECs (Fig. 7) where TECs are ~100 times more sensitive to DOX. These calculations explain the better therapeutic efficacy of large size RGD-PEG-LP for the treatment of RCC. Due to the resistance of RCC, DOX is not used clinically. However, this study outlines a potential approach for treating RCC by utilizing DOX loaded nanoparticles via the targeting of tumor vessels.

5. Conclusions

Collectively, small size PEG-LPs (either Doxil or RGD-PEG-LP) extravasate to

DOX resistant tumor cells via the EPR effect, where the large size RGD-PEG-LP (DOX) can minimize the EPR effect and specifically bind to and kill the TECs, a process called the anti-angiogenic effect. This then leads to the death of angiogenesis dependent tumor cells. Therefore, the anti-tumor activity of the large size RGD-PEG-LP (DOX) at its lower dose against RCC tumors can be ascribed to the selective targeting and apoptosis of TECs (OSRC-ECs) and destruction of the tumor vasculature rather than having a direct effect on drug resistant OSRC-2 cells. For targeting TECs in drug-resistant cancer, the large size particle shows more promise than the small size version, because of its higher targetability and drug delivery efficiency to TECs. Even though; large size particles remained beyond the interest of use, our results show an application of such particles in cancer therapy, indicating the shift of paradigm. The results obtained in this study revealed an effective anti-angiogenic therapy mediated by controlling the size of the nanoparticles for the treatment of drug-resistant, rapidly growing kidney cancer, indicating an attractive approach for future clinical trials.

Conflict of interest

The authors have no potential conflicts of interest to disclose.

Acknowledgements

This study was supported in parts by grants from the Special Education and Research Expenses of the Ministry of Education, Culture, Sports, Science and Technology of Japan (MEXT); as well as by a Grant-in-Aid for Research on Medical Device Development from the Ministry of Health, Labour and Welfare of Japan (MHLW). We thank Dr. Milton S. Feather for editing the manuscript.

References

[1] Slingerland M, Guchelaar HJ, Gelderblom H. Liposomal drug formulations in cancer therapy: 15 years along the road. Drug Discov Today 2012;17:160-6.

[2] Haley B, Frenkel E. Nanoparticles for drug delivery in cancer treatment. Urol Oncol 2008,26:57-64.

[3] Maeda H, Wu J, Sawa T, Matsumura Y, Hori K. Tumor vascular permeability and the EPR effect in macromolecular therapeutics: a review. J Control Release 2000,65:271-84.

[4] Yuan F, Leunig M, Huang SK, Berk DA, Papahadjopoulos D, Jain RK. Microvascular permeability and interstitial penetration of sterically stabilized (Stealth®) liposomes in a human tumor xenografts. Cancer Res 1994,54: 3352-56.

[5] Pastorino F, Brignole C, Marimpietri D, Cilli M, Gambini C, Ribatti D, et al. Vascular damage and anti-angiogenic effects of tumor vessel-targeted liposomal chemotherapy. Cancer Res 2003;63:7400-9.

[6] Murphy EA, Majeti BK, Barnes LA, Makale M, Weis SM, Lutu-Fuga K, et al. Nanoparticle-mediated drug delivery to tumor vasculature suppresses metastasis. Proc Natl Acad Sci USA 2008;105:9343-8.

[7] Schiffelers RM, Koning GA, ten Hagen TL, Fens MH, Schraa AJ, Janssen AP, et al. Anti-tumor efficacy of tumor vasculature-targeted liposomal doxorubicin. J Control Release 2003;91:115-22.

[8] Pastorino F, Brignole C, Marimpietri D, Sapra P, Moase EH, Allen TM, Ponzoni M. Doxorubicin-loaded Fab' fragments of anti-disialoganglioside immunoliposomes selectively inhibit the growth and dissemination of human neuroblastoma in nude mice. Cancer Res 2003;63:86-92.

[9] Poljaková J, Eckschlager T, Hřebačková J, Hraběta J, Stiborová M. The

comparison of cytotoxicity of the anticancer drugs doxorubicin and ellipticine to human neuroblastoma cells. Interdiscip Toxicol 2008;1:186-9.

[10] Park J, Bae E, Lee C, Yoon SS, Chae YS, Ahn KS, Won NH. RNA interference-directed caveolin-1 knockdown sensitizes SN12CPM6 cells to doxorubicin-induced apoptosis and reduces lung metastasis. Tumour Biol 2010;31:643-50.

[11] Burg MA, Pasqualini R, Arap W, Ruoslahti E, Stallcup WB. NG2 proteoglycan-binding peptides target tumor neovasculature. Cancer Res 1999;59:2869-74.

[12] Kondo M, Asai T, Katanasaka Y, Sadzuka Y, Tsukada H, Ogino K, et al. Anti-neovascular therapy by liposomal drug targeted to membrane type-1 matrix metalloproteinase. Int J Cancer 2004;108:301-6.

[13] Oku N, Asai T, Watanabe K, Kuromi K, Nagatsuka M, Kurohane K, et al. Anti-neovascular therapy using novel peptides homing to angiogenic vessels. Oncogene 2002;21:2662-9.

[14] Hashizume H, Baluk P, Morikawa S, McLean JW, Thurston G, Roberge S, et al. Openings between defective endothelial cells explain tumor vessel leakiness. Am J Pathol 2000;156:1363-80.

[15] Drummond DC, Meyer O, Hong K, Kirpotin DB, Papahadjopoulos D. Optimizing liposomes for delivery of chemotherapeutic agents to solid tumors. Pharmacol Rev 1999;51:691-743.

[16] Decuzzi P, Godin B, Tanaka T, Lee SY, Chiappini C, Liu X, et al. Size and shape effects in the biodistribution of intravascularly injected particles. J Control Release 2010;141:320-7.

[17] Gentile F, Curcio A, Indolfi C, Ferrari M, Decuzzi P. The margination propensity of spherical particles for vascular targeting in the

microcirculation. J Nanobiotechnology 2008:6:9.

[18] Haun JB, Hammer DA. Quantifying nanoparticle adhesion mediated by specific molecular interactions. Langmuir 2008;24:8821-32.

[19] Liu D, Mori A, Huang L. Role of liposome size and RES blockade in controlling biodistribution and tumor uptake of GM1-containing liposomes. Biochim Biophys Acta 1992;1104:95-101.

[20] Maruyama K, Yuda T, Okamoto A, Kojima S, Suginaka A, Iwatsuru M. Prolonged circulation time in vivo of large unilamellar liposomes composed of distearoyl phosphatidylcholine and cholesterol containing amphipathic poly(ethylene glycol). Biochim Biophys Acta 1992;1128:44-9.

[21] Litzinger DC, Buiting AM, van Rooijen N, Huang L. Effect of liposome size on the circulation time and intraorgan distribution of amphipathic poly(ethylene glycol)-containing liposomes. Biochim Biophys Acta 1994;1190:99-107.

[22] Kibria G, Hatakeyama H, Ohga N, Hida K, Harashima H. Dual-ligand modification of PEGylated liposomes shows better cell selectivity and efficient gene delivery. J Control Release 2011,153:141-8.

[23] Vogelzang NJ, Stadler WM. Kidney cancer. Lancet 1998;352:1691-96.

[24] Efferth T, Volm M. Protein expression profiles indicative for drug resistance of kidney carcinoma. Cancer Genomics & Proteomics 2004;1:17-22.

[25] Mourad WF, Dutcher J, Ennis RD. State-of-the-Art management of renal cell carcinoma. Am J Clin Oncol 2012 Aug 2. (Epub ahead of print)

[26] Staehler M, Rohrmann K, Bachmann A, Zaak D, Stief CG, Siebels M. Therapeutic approaches in metastatic renal cell carcinoma. BJU Int 2005;95:1153-61.

[27] Soto-Vega E, Arroyo C, Richaud-Patin Y, García-Carrasco M, Vázquez-Lavista LG, Llorente L. P-glycoprotein activity in renal clear cell carcinoma. Urol

Oncol 2009;27:363-66.

[28] Shimizu K, Oku N. Cancer anti-angiogenic therapy. Biol Pharm Bull 2004,27:599-605.

[29] Hida K, Hida Y, Shindoh M. Understanding tumor endothelial cell abnormalities to develop ideal anti-angiogenic therapies. Cancer Sci 2008;99:459-66.

[30] Kaelin WG Jr. The von Hippel-Lindau tumor suppressor gene and kidney cancer. Clin Cancer Res 2004;10:6290S–6295S.

[31] Hutson TE. Targeted therapies for the treatment of metastatic renal cell carcinoma: clinical evidence. The Oncologist 2011;16:14-22.

[32] Di Lorenzo G, Buonerba C, Biglietto M, Scognamiglio F, Chiurazzi B, Riccardi F, et al. The therapy of kidney cancer with biomolecular drugs. Cancer Treat Rev 2010:36S3:S16-20.

[33] Zhang L, Bhasin M, Schor-Bardach R, Wang X, Collins MP, Panka D, et al. Resistance of renal cell carcinoma to sorafenib is mediated by potentially reversible gene expression. PLoS One 2011;6:e19144.

[34] Huang D, Ding Y, Zhou M, Rini BI, Petillo D, Qian CN, et al. Interleukin-8 mediates resistance to antiangiogenic agent sunitinib in renal cell carcinoma. Cancer Res 2010;70:1063-71.

[35] Hammers HJ, Verheul HM, Salumbides B, Sharma R, Rudek M, Jaspers J, et al. Reversible epithelial to mesenchymal transition and acquired resistance to sunitinib in patients with renal cell carcinoma: evidence from a xenograft study. Mol Cancer Ther 2010;9:1525-35.

[36] Di Lorenzo G, Porta C, Bellmunt J, Sternberg C, Kirkali Z, Staehler M,et al. Toxicities of targeted therapy and their management in kidney cancer. Eur Urol 2011;59:526-40.

[37] Takara K, Hatakeyama H, Kibria G, Ohga N, Hida K, Harashima H. Size-controlled, dual-ligand modified liposomes that target the tumor vasculature show promise for use in drug-resistant cancer therapy. J Control Release 2012;162:225-232.

[38] Matsuda K, Ohga N, Hida Y, Muraki C, Tsuchiya K, Kurosu T, et al. Isolated tumor endothelial cells maintain specific character during long-term culture. Biochem Biophys Res Commun 2010;394:947-54.

[39] Akino T, Hida K, Hida Y, Tsuchiya K, Freedman D, Muraki C, et al. Cytogenetic abnormalities of tumor-associated endothelial cells in human malignant tumors. Am J Pathol 2009;175:2657-67.

[40] Tsuchiya K, Hida K, Hida Y, Muraki C, Ohga N, Akino T, et al. Adrenomedullin antagonist suppresses tumor formation in renal cell carcinoma through inhibitory effects on tumor endothelial cells and endothelial progenitor mobilization. Int J Oncol 2010;36:1379-86.

[41] Fritze A, Hens F, Kimpfler A, Schubert R, Peschka-Süss R. Remote loading of doxorubicin into liposomes driven by a transmembrane phosphate gradient. Biochim Biophys Acta 2006;1758:1633-40.

[42] Haran G, Cohen R, Bar LK, Barenholz Y. Transmembrane ammonium sulfate gradient in liposomes produce efficient and stable entrapment of amphipathic weak bases. Biochim Biophys Acta 1993;1151:201-15.

[43] Enoch HG, Strittmatter P. Formation and properties of 1000-A-diameter, single-bilayer phospholipid vesicles. Proc Natl Acad Sci USA 1979;76:145-9.

[44] Xu X, Khan MA, Burgess DJ. Predicting hydrophilic drug encapsulation inside unilamellar liposomes. Int J Pharm 2012;423:410-8.

[45] A mathematical model to predict drug encapsulation inside liposomes. Available from URL: http://www.liposomemodel.com.

[46] Ogawara K, Un K, Tanaka K, Higaki K, Kimura T. In vivo anti-tumor effect of PEG liposomal doxorubicin (DOX) in DOX-resistant tumor-bearing mice: involvement of cytotoxic effect on vascular endothelial cells. J Control Release 2009;133:4-10.

[47] Montet X, Funovics M, Montet-Abou K, Weissleder R, Josephson L. Multivalent effects of RGD peptides obtained by nanoparticle display. J Med Chem 2006;49:6087-93.

[48] Singh B, Rawlings N, Kaur A. Expression of integrin alphavbeta3 in pig, dog and cattle. Histol Histopathol 2001;16:1037-46.

[49] Singh B, Fu C, Bhattacharya J. Vascular expression of the alpha(v)beta(3)-integrin in lung and other organs. Am J Physiol Lung Cell Mol Physiol 2000;278:L217-26.

[50] Pastorino F, Brignole C, Di Paolo D, Nico B, Pezzolo A, Marimpietri D, et al. Targeting liposomal chemotherapy via both tumor cell-specific and tumor vasculature-specific ligands potentiates therapeutic efficacy. Cancer Res 2006;66:10073-82.

[51] Wang Z, Yu Y, Dai W, Lu J, Cui J, Wu H, et al. The use of a tumor metastasis targeting peptide to deliver doxorubicin-containing liposomes to highly metastatic cancer. Biomaterials 2012;33:8451-60.

[52] Du B, Han H, Wang Z, Kuang L, Wang L, Yu L, et al. Targeted drug delivery to hepatocarcinoma in vivo by phage-displayed specific binding peptide. Mol Cancer Res 2010;8:135-44.

[53] Zheng JY, Chen D, Chan J, Yu D, Ko E, Pang S. Regression of prostate cancer xenografts by a lentiviral vector specifically expressing diphtheria toxin A. Cancer Gene Ther 2003;10:764-70.

[54] Dass CR, Choong PF. Targeting of small molecule anticancer drugs to the

tumour and its vasculature using cationic liposomes: lessons from gene therapy. Cancer Cell Int 2006;6:17.

[55] Folkman J. Angiogenesis in cancer, vascular, rheumatoid and other disease. Nat Med 1995;1:27-31.

[56] Molema G, Meijer DL, de Leij LF. Tumor vasculature targeted therapies: getting the players organized. Biochem Pharmacol 1998;55:1939-45.

Tables

Table 1: Physical properties of size controlled PEG-LPs prepared using EPC, Cholesterol as lipid components. The data are expressed as the mean±SD value from at least six different preparations. Size dependent binding of RGD-PEG-LPs with Integrin αvβ3 receptor expressing from HUVEC. Different lipid doses of RGD-PEG-LPs was added to 40,000 cells and incubated for 2 h at 4 ^{0}C and 37 ^{0}C. Kd and Bmax values were calculated using the Sigma-plot software. The results expressed as the mean±SD, n=3-4.

Sample ID		Diameter (nm)	Poly dispersity index (PDI)	Zeta-potential (mV)	Binding constant (Kd value); (no. of particles x 10^{10}/well)		Binding maximum (Bmax); (maximum fluorescence intensity)	
					4 ^{0}C	37 ^{0}C	4 ^{0}C	37 ^{0}C
Small size	PEG-LP	121±10	0.12±0.00	-12±7	-	-	-	-
	RGD-PEG-LP	127±2	0.13±0.01	-19±3	2.46±0.39	6.96±2.68	79.4±31.5	223.2±42.7
Large size	PEG-LP	327±8	0.20±0.06	-13±5	-	-	-	-
	RGD-PEG-LP	326±11	0.19±0.03	-16±8	0.25±0.11	0.62±0.52	92.4±21.1	203.3±51.8
Relative binding efficiency of large size RGD-PEG-LP (vs small size)					9.70±2.8	11.2±6.0	-	-

Figure Captions

Fig. 1. Size dependent cellular uptake of PEG-LPs in HUVEC.

Small and large size PEG-LPs were prepared by lipid film hydration method followed by extrusion to control the size. Size distribution of PEG-LPs was obtained by the DLS measurement (A). Forty thousand cells were incubated with rhodamine labeled PEG-LPs for 2 h at 37 °C and observed under CLSM (B). Area of internalized PEG-LPs (C), as counted from 100, 90, 97 and 105 cells treated with small size PEG, small size RGD, large size PEG and large size RGD, respectively (in at least 15 images/group). Cellular uptake based on the binding of RGD-PEG-LPs to Integrin $\alpha v\beta 3$ receptor expressed by HUVEC following a 2 h incubation at 4 °C and 37 °C (D); small size RGD-PEG-LP (square, open), large size RGD-PEG-LP (square, close), mean±SD, n=3-4. Statistical analysis was done by unpaired t-test (**P<0.01). Inhibition of cellular uptake of RGD-PEG-LPs in presence of free RGD (E). Twenty five thousand cells were incubated with different concentrations of free RGD for 5 min at 37 °C followed by incubation with rhodamine labeled RGD-PEG-LPs for 20 min at 37 °C and observed under CLSM. Blue: DAPI, scale bars 20 μm. Schematic representations of the multivalent interactions of RGD molecules with its target receptor (F), where RGD is present on the top of PEG of either small or large size PEG-LP.

Fig. 2. Distribution of size-controlled PEG-LPs in RCC tumor tissues.

Radio-labeled PEG-LPs were injected to mice (n=4) and radioactivity was measured at 24 h post-injection (A); PEG-LPs (□), RGD-PEG-LPs (■). Data presented as mean±SD. Statistical analyses involved the two-tail unpaired t-test. Small PEG vs small RGD $^{\#}$P<0.05; large PEG vs large RGD *P<0.05. Rhodamine labeled PEG-LPs were injected to mice (0.5 μmol lipid/mouse). Representative images of tumors collected at 6 h post-injection are shown (B), green: tumor vessel, blue: DAPI. Small size PEG-LP was detected through out the tumor, large size RGD-PEG-LP was mostly found along with tumor vessels where it merged (arrows). Scale bars 50 μm. Original images were given in supplementary Fig. S2.

Fig. 3. Therapeutic effect of DOX loaded PEG-LPs in RCC tumor bearing mice. Mice were treated with 1.5 mg/kg DOX in PEG-LPs or with PBS (control). Data presented as mean±SD (n=4-5). Statistical analysis was done by One-way ANOVA followed by SNK-test. **P<0.01; N.S., not significant.

Fig. 4. Site of action and blood vessel disruption effect of DOX loaded size controlled PEG-LPs in tumor. Mice bearing RCC tumors were treated with 1.5 mg/kg DOX (n=3) in PEG-LPs or with PBS. At 24 h post-injection, tumors were collected and analyzed under CLSM. To detect apoptosis in tumors, mice were injected with Apo-Trace solution (A), red: tumor vessel, green: apoptotic cells, arrows: apoptotic endothelial cells. Total area of apoptotic cells (B) and area of apoptotic endothelial cells (C) was counted from at least 35 images taken from different positions in tumors/treated group. Morphology of tumor vessels (D); area of tumor vessel (E), nuclei (F) were counted from 20758, 19544, 17873 and 14769 cells in 30-50 images taken from different positions of the tumors treated with PBS, DOX loaded small size PEG-LP, small size RGD-PEG-LP and large size RGD-PEG-LP, respectively. Scale bars; 50 μm. Statistical analysis was done by Bonferroni One-way ANOVA followed by SNK-test (B), Dunnett-test (E, F); and unpaired t-test (C). *P<0.05; **P<0.01; N.S, not significant.

Fig. 5. Cytotoxicity study of tumor cells and tumor endothelial cells using free DOX. OSRC-2 and OSRC-ECs recovered from OSRC-2 tumor tissue were incubated with free DOX for 8 h followed by 18 h reincubation and cell counting (A). Cells were treated with 10 μg/ml of DOX for 8 h and amount of internalized DOX was calculated (B). Data presented as mean±SD, n=3-4. Statistical analysis was done by unpaired t-test (**P<0.01).

Fig. 6. Observation of the morphology of normal blood vessels treated with PEG-LPs (DOX). Confocal images of normal organs from mice bearing OSRC-2 tumor were treated with PBS (control) or three consecutive once daily dose of 1.5 mg/kg doxorubicin (i.v. injection via tail vein) in PEG-LPs. At 24 h post-injection, the animals were sacrificed; organs were collected and stained with FITC-Isolectin (for blood vessel) and Hoechst 33342 (for nuclei) followed by analysis under CLSM. Representative images from three independently studied mice for each PEG-LP (DOX) are shown (A). Simultaneously, blood sample was collected and toxicological study was performed by measuring the serum ALT (B) and AST (C) level. Data are presented as the mean±SD. Statistical analysis vs control was performed by One-way ANOVA followed by Dunnett-test. N.S., not significant.

Fig. 7. Comparisons describing the therapeutic efficacy of large size RGD-PEG-LP (DOX) over Doxil in RCC tumor. Doxil (small size PEG-LP, ~100 dnm) extravasates to tumor cells (OSRC-2) which are resistant to DOX. Large size RGD-PEG-LP (~300 dnm) minimizes the extravasation and preferentially targets the TECs (OSRC-EC) which are ~100 times more sensitive to DOX. Compared to DOX delivered by Doxil to tumor cells, about 40 times higher amount of DOX could be delivered by large size RGD-PEG-LP to TECs indicating its efficiency for the treatment of RCC.

Fig. 1.

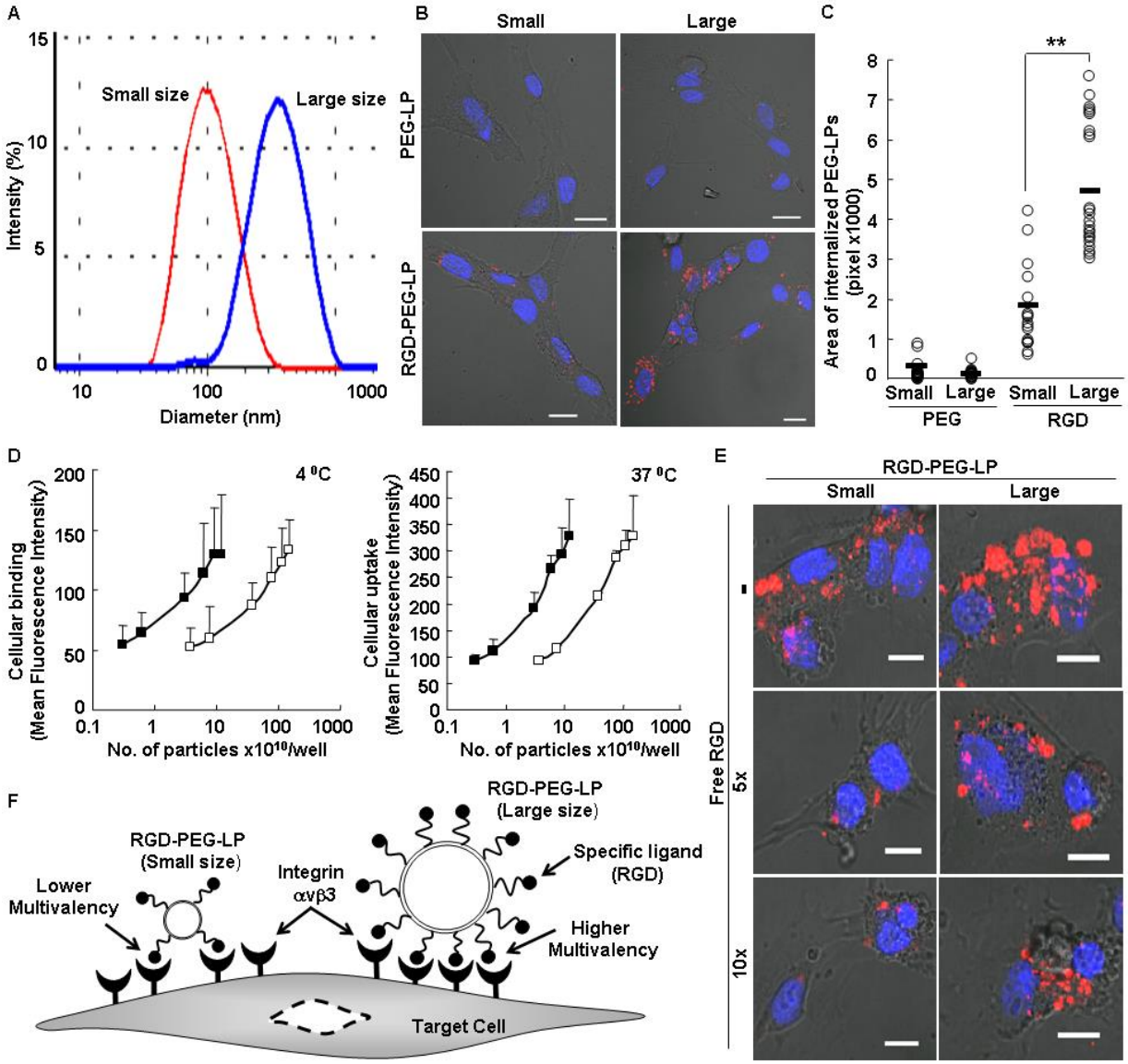

A
Small size
Large size
Intensity (%)
Diameter (nm)
B
Small
Large
PEG-LP
RGD-PEG-LP
C
Area of internalized PEG-LPs (pixel x1000)
**
Small
Large
Small
Large
PEG
RGD
D
4 °C
37 °C
Cellular binding (Mean Fluorescence Intensity)
Cellular uptake (Mean Fluorescence Intensity)
No. of particles x10¹⁰/well
No. of particles x10¹⁰/well
E
RGD-PEG-LP
Small
Large
Free RGD
-
5x
10x
F
RGD-PEG-LP (Small size)
RGD-PEG-LP (Large size)
Lower Multivalency
Integrin αvβ3
Specific ligand (RGD)
Higher Multivalency
Target Cell

Fig. 2.

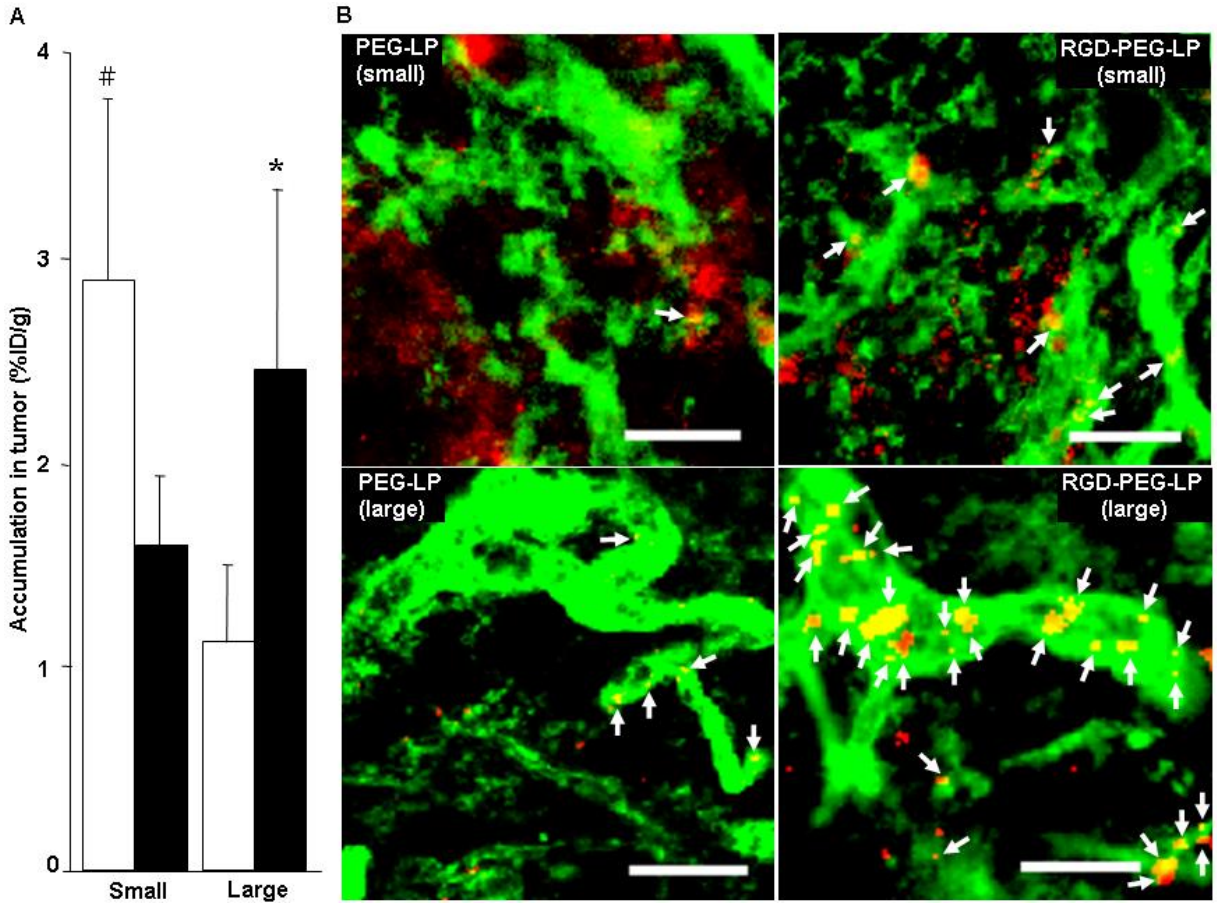

A
B
4
3
2
1
0
#
*
Accumulation in tumor (%ID/g)
Small
Large
PEG-LP
(small)
RGD-PEG-LP
(small)
PEG-LP
(large)
RGD-PEG-LP
(large)

Fig. 3.

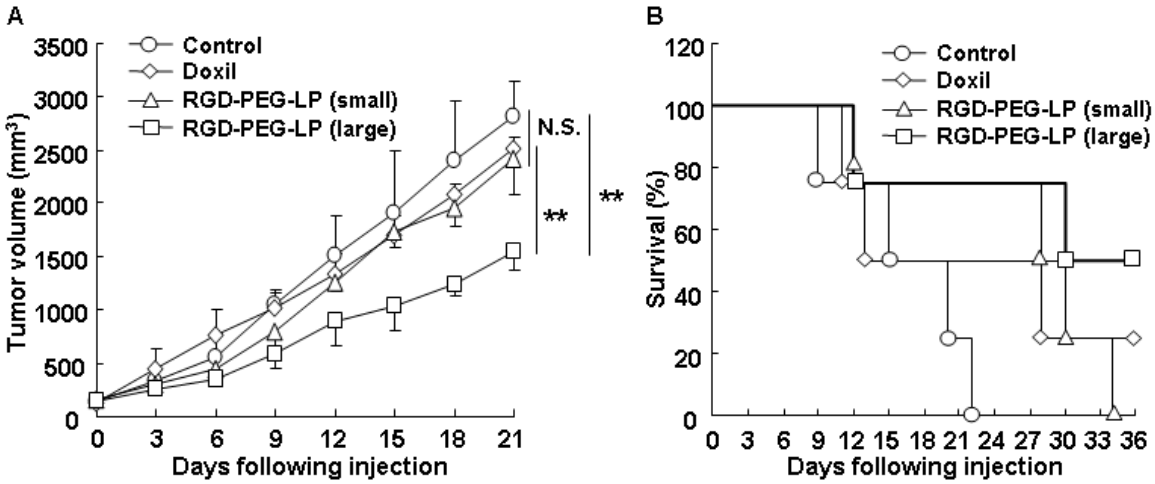

A
Control
Doxil
RGD-PEG-LP (small)
RGD-PEG-LP (large)
Tumor volume (mm3)
3500
3000
2500
2000
1500
1000
500
0
0 3 6 9 12 15 18 21
Days following injection
N.S.
**
**
B
Control
Doxil
RGD-PEG-LP (small)
RGD-PEG-LP (large)
Survival (%)
120
100
80
60
40
20
0
0 3 6 9 12 15 18 21 24 27 30 33 36
Days following injection

Fig. 4.

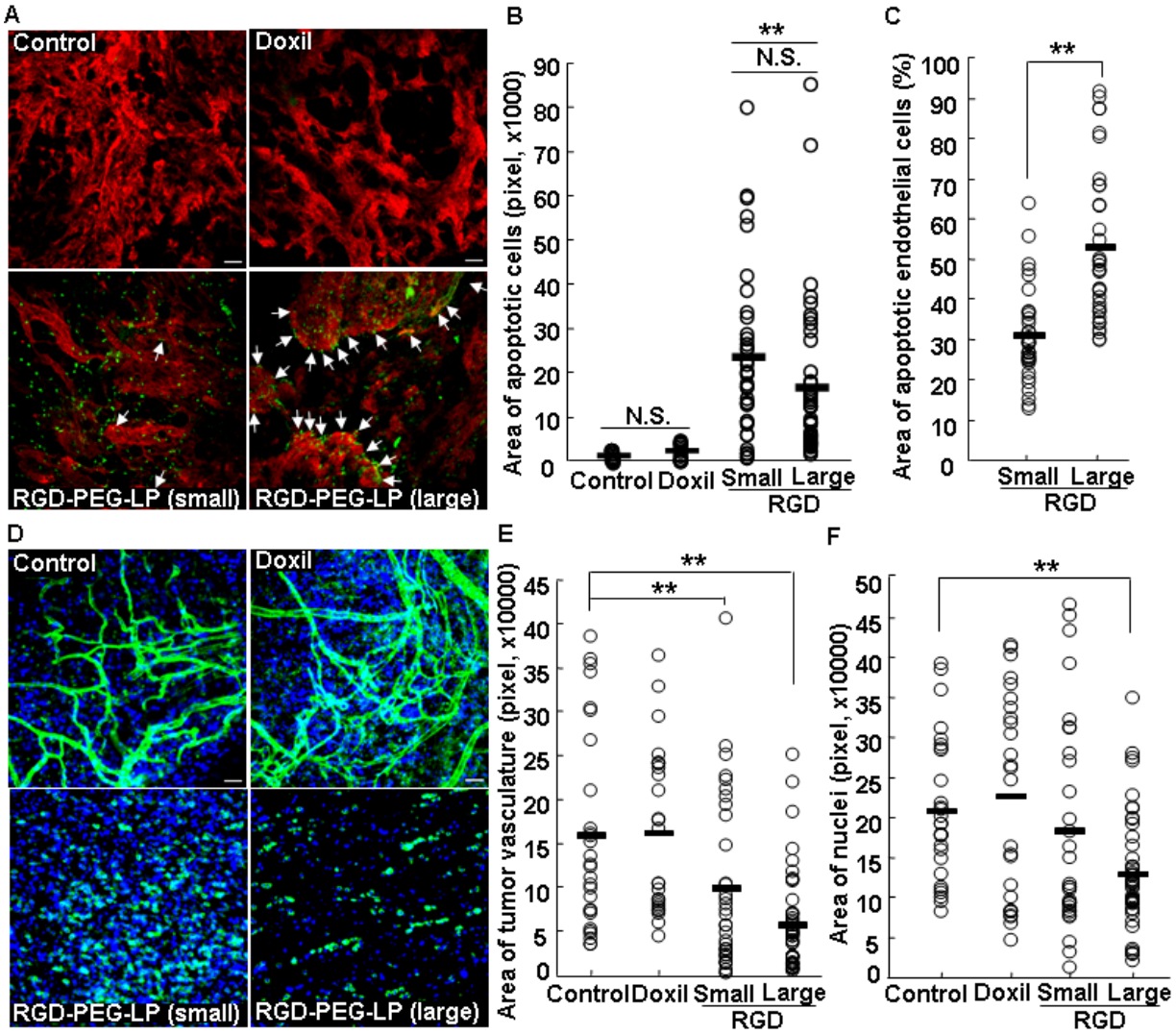

A
Control
Doxil
RGD-PEG-LP (small)
RGD-PEG-LP (large)
B
Area of apoptotic cells (pixel, x1000)
N.S.
**
N.S.
Control
Doxil
Small
Large
RGD
C
Area of apoptotic endothelial cells (%)
**
Small
Large
RGD
D
Control
Doxil
RGD-PEG-LP (small)
RGD-PEG-LP (large)
E
Area of tumor vasculature (pixel, x10000)
**
**
Control
Doxil
Small
Large
RGD
F
Area of nuclei (pixel, x10000)
**
Control
Doxil
Small
Large
RGD

Fig. 5.

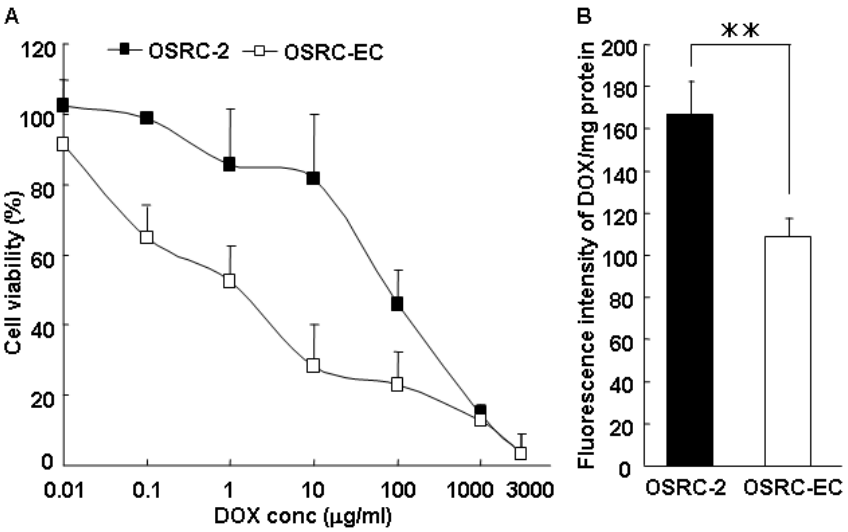

A
OSRC-2
OSRC-EC
Cell viability (%)
120
100
80
60
40
20
0
0.01
0.1
1
10
100
1000
3000
DOX conc (μg/ml)
B
**
Fluorescence intensity of DOX/mg protein
200
180
160
140
120
100
80
60
40
20
0
OSRC-2
OSRC-EC

Fig. 6.

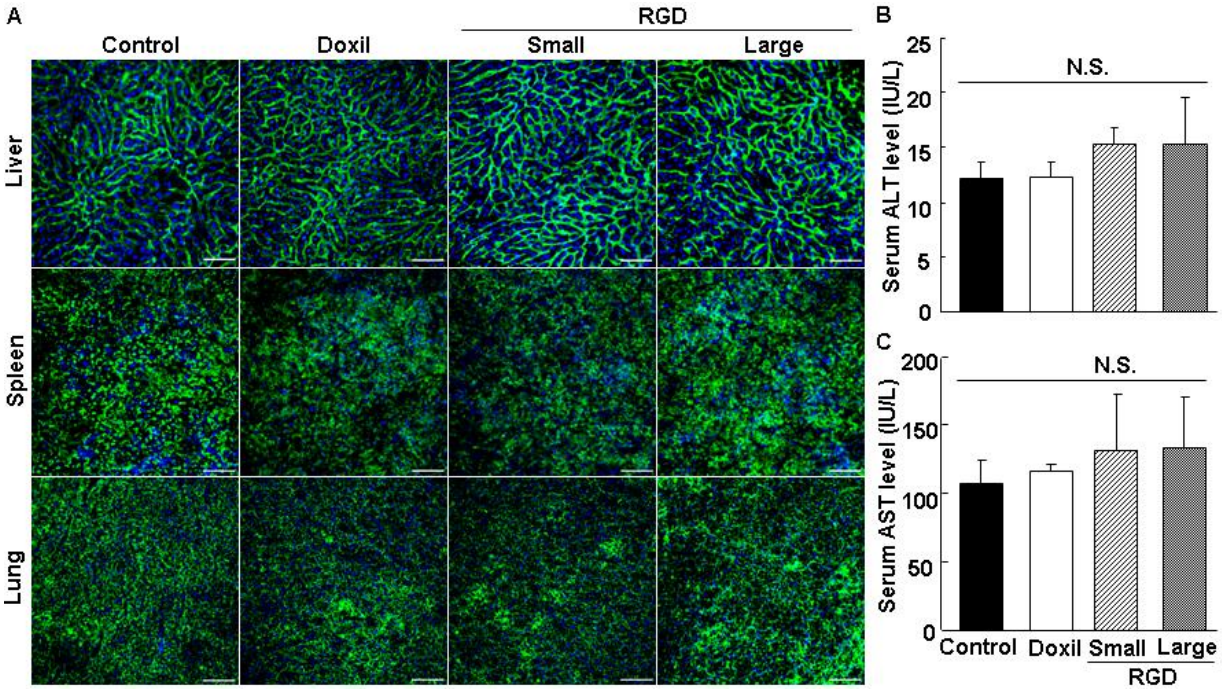
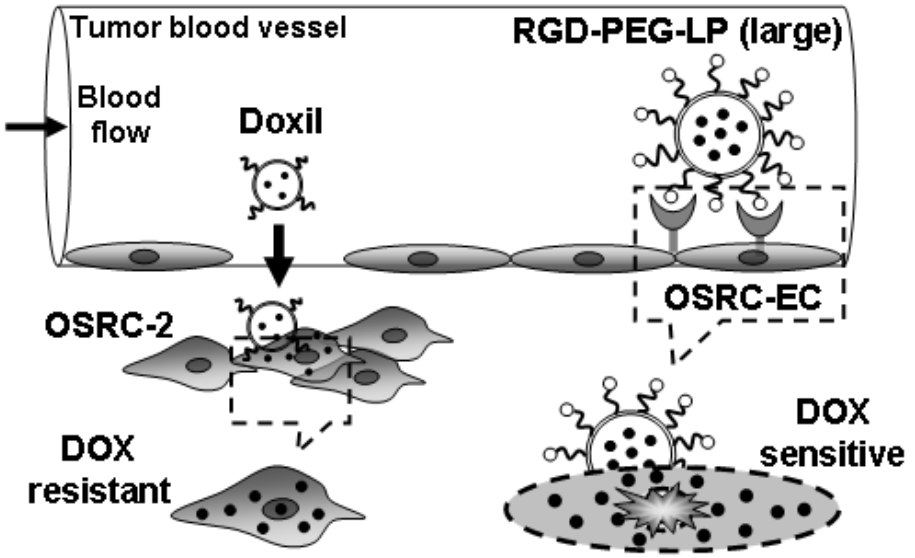

A
RGD
Control
Doxil
Small
Large
Liver
Spleen
Lung
B
N.S.
Serum ALT level (IU/L)
25
20
15
10
5
0
C
N.S.
Serum AST level (IU/L)
200
150
100
50
0
Control
Doxil
Small
Large
RGD

Fig. 7.



Parameters	Doxil	RGD-PEG-LP (large)	Relative value (vs tumor cell)
Target site	OSRC-2	OSRC-EC	-
No. of cell	10^8/g tumor	$2x10^6$/g tumor	-
Injected DOX (total)	3 μg/mouse	3 μg/mouse	-
Delivered DOX dose (%)	3% ID/g tumor	2.5% ID/g tumor	
Delivered DOX /cell	$90x10^{-8}$ ng	$37.5x10^{-6}$ ng	40
DOX sensitivity (EC_{50})	100 μg/ml	1 μg/ml	100

Supplementary Data

Preparation of DOX loaded PEG-LPs for therapeutic applications

LPs composed of HSPC and Cholesterol (molar ratio: 7/3) were prepared by the lipid film hydration method. After evaporation under a stream of nitrogen gas, the dried lipid films were hydrated with 155 mM ammonium sulfate (pH 5.5) followed by incubation at 70 °C and vortex. The prepared LPs were extruded through 0.4 μm filter to control the size. The external phase of the LPs was replaced with PBS (pH 7.4) by gel filtration with a Sephadex G-25 column (GE Healthcare Ltd.). Doxorubicin (DOX) was loaded into the LPs via an ammonium sulfate gradient, as reported in ref. 1-2. DOX in PBS (pH 8.0) was added to the LPs at a drug-to-lipid molar ratio of 1:10 and incubated at 60 °C for 1 h and free DOX was removed by filtering the LPs using Amicon 50,000 MWCO filter. DOX content in LPs was determined by disintegration of the liposomal bilayer in methanol and colorimetric determination of doxorubicin concentration. Five mol% PEG-DSPE or RGD-PEG-DSPE was incorporated into the lipid membrane of the LPs by incubating at 60 °C for 30 min to prepare PEG-LP (DOX) or RGD-PEG-LP (DOX) respectively. For small size LP, lipid film was hydrated with 155 mM ammonium sulfate followed by probe sonication. DOX loading and RGD-PEG modification was accomplished by the above procedure to prepare small size RGD-PEG-LP (DOX). In the case of Doxil, a lipid film was prepared by using HSPC/Cholesterol (molar ratio: 3/2) and 5.3 mol% PEG-DSPE. Lipid film was hydrated with 155 mM ammonium sulfate for 15 min followed by probe sonication. DOX was loaded by following the above procedure.

In vitro delivery of DOX to target cells by PEG-LPs

To observe the cellular uptake of DOX, 75000 HUVEC cells were seeded on a 35-mm glass-bottom dish in 2 ml of culture medium for 24 h. On the next day, 10 μg/ml of doxorubicin (as free drug or encapsulated within the PEG-LPs) in cell culture media was added to cells and incubated for 30 min at 37 °C. After 20 min of incubation, 5 μl of Hoechst 33342 (1 mg/ml) was added to stain the nuclei and the suspension was reincubated for an additional 10 min. The medium was then removed followed by washing twice with PBS. Finally, 1 ml of Krebs buffer was added and the cells were observed under CLSM.

Biodistribution of PEG-LPs in tumor-bearing mice

To assess the tissue distribution of PEG-LPs, male BALB/c nude mice (n=4) were inoculated subcutaneously with $2x10^6$ OSRC-2 cells in 70 μL PBS. At a tumor volume of 200-250 mm^3, mice were intravenously injected via the tail vein with ^{3}H-CHE-labeled PEG-LPs at a dose of 0.5 μmol lipid/200 μl injection volume. At 24 h after injection, animals were sacrificed; blood and other organs were collected and weighed. After weighing, the samples were solubilized in Soluene-350 (PerkinElmer Life Sciences) for 5 h at 50 °C. Blood samples were decolorized by treatment with H_2O_2. The radioactivities of the samples were measured using a liquid scintillation counter (LSC-6100, Aloka) after adding 10 ml of Hionic Flour (Perkin-Elmer Life Sciences). The blood concentration and tissue accumulation of LPs were represented as the % of injected dose (ID) per ml of blood and %ID per g tissue, respectively. To elucidate the distribution of PEG-LPs in each tissue (Xtissue), the following equation was followed where the radioactivities in various organ samples (Xorgan) were measured and minimized by the concentration of PEG-LPs in the vascular space, as described in ref. 3.

$X_{tissue} = X_{organ} - V_0C(t)$

where V_0 denotes the total volume of the vascular space and interstitial fluid and C(t) is plasma concentration.

1. Fritze A, Hens F, Kimpfler A, Schubert R, Peschka-Süss R. Remote loading of doxorubicin into liposomes driven by a transmembrane phosphate gradient. Biochim Biophys Acta 2006;1758:1633-40.
2. Haran G, Cohen R, Bar LK, Barenholz Y. Transmembrane ammonium sulfate gradient in liposomes produce efficient and stable entrapment of amphipathic weak bases. Biochim Biophys Acta 1993;1151:201-15.
3. Hatakeyama H, Akita H, Maruyama K, Suhara T, Harashima H. Factors governing the in vivo tissue uptake of transferrin-coupled polyethylene glycol liposomes in vivo. Int J Pharm 2004;281:25-33.
4. Singh B, Rawlings N, Kaur A. Expression of Integrin alphavbeta3 in pig, dog and cattle. Histol Histopathol 2001;16:1037-46.

Supplementary Figures

Fig. S1. Biodistribution of PEG-LPs in RCC tumor bearing mice. OSRC-2 tumor bearing mice (n=4) were injected intravenously with radio-labeled PEG-LPs as described in the material and methods section. At 24 h post-injection, organs were collected and analyzed for radioactivity (A); PEG-LPs (□), RGD-PEG-LPs (■). Higher amounts of small size PEG-LP were found in blood due to its long circulation property, which is mediated by PEGylation. However, the blood concentration of large size PEG-LP was lower, which can be attributed to entrapment of the particles in the splenic filter. On the other hand, both small and large size RGD-PEG-LPs were rapidly cleared from the blood which can be attributed to their recognition by Integrin $\alpha v\beta 3$ expressed from phagocytes in the spleen, as described in ref. 4. In liver, about 40-50% of the injected dose/g tissue of small size PEG-LP or RGD-PEG-LP was accumulated. Compared to small PEG-LP, the accumulation of large size PEG-LP was found relatively lower. However, RGD modification significantly increased the accumulation of large size PEG-LPs by the liver, which could be attributed to its possible interaction with receptors expressed from liver sinusoidal endothelial cells or recognition by RES. Very small amounts of the small PEG-LP had accumulated in the spleen where it can pass through the splenic filter; however, RGD modification significantly increased the accumulation of small size PEG-LP. Conversely, large size PEG-LP accumulated more rapidly in the spleen where it is trapped by the splenic filter and no significant difference in accumulation was observed from large size RGD-PEG-LP. In lungs, nearly the same amounts of small size PEG-LP and small size RGD-PEG-LP had accumulated. However, RGD modification significantly enhances the lung accumulation of large size PEG-LP. Few amounts of PEG-LPs were accumulated in other organs. Data are presented as mean±SD. Statistical analysis was performed by two-tail unpaired t-test. Small PEG vs small RGD $^{\#\#}P<0.01$; large PEG vs large RGD $^{*}P<0.05$, $^{**}P<0.01$; N.S, not significant. Total recovery of PEG-LPs obtained in biodistribution study was counted (B).

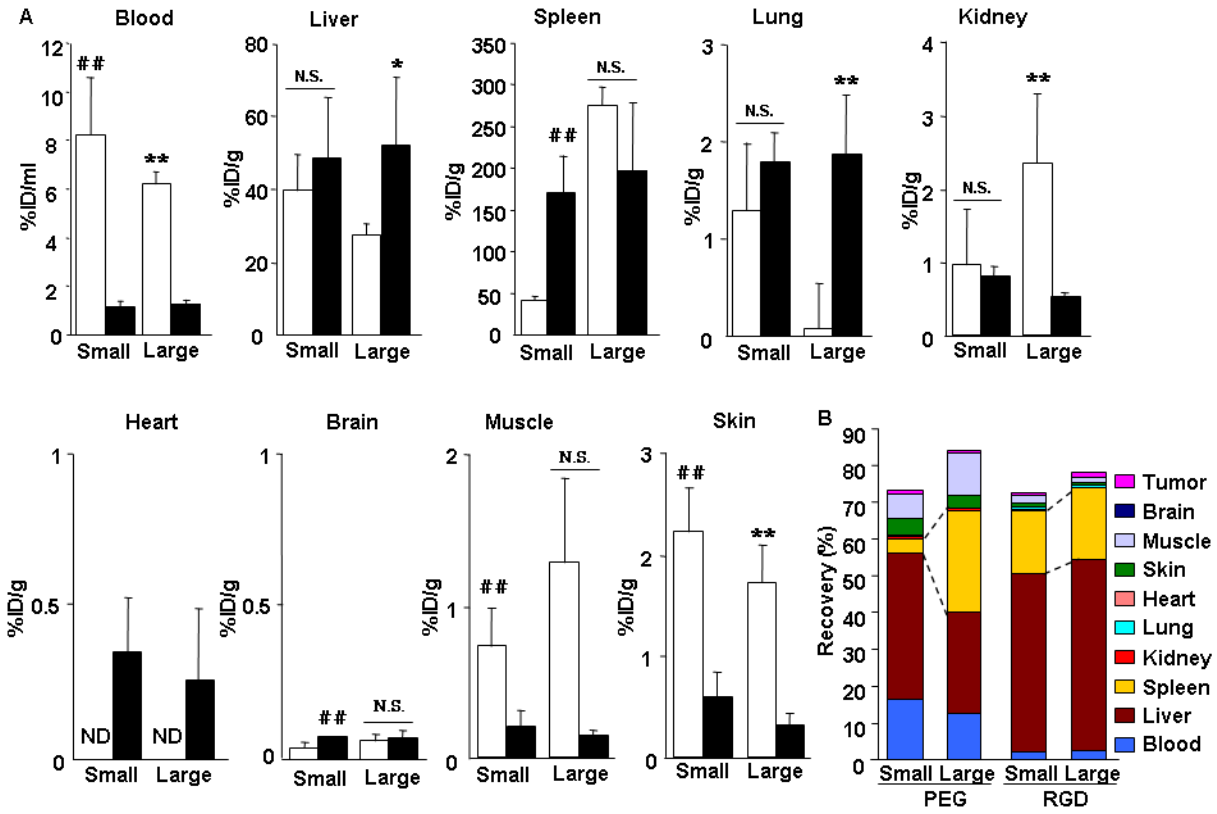

A
Blood
Liver
Spleen
Lung
Kidney
%ID/ml
%ID/g
##
**
N.S.
*
Small
Large
Heart
Brain
Muscle
Skin
ND
B
Recovery (%)
Tumor
Brain
Muscle
Skin
Heart
Lung
Kidney
Spleen
Liver
Blood
PEG
RGD

Fig. S2. Size dependent distribution of PEG-LPs in the tumor microenvironment.
Rhodamine labeled PEG-LPs were injected into RCC tumor bearing mice (0.5 μmol lipid/mouse). Representative images of tumors collected at 6 h post-injection are shown, green: tumor vessel, red: PEG-LP. Small size PEG-LP was detected through out the tumor where it mostly extravasated to tumor cells, a process called the EPR effect. Small size RGD-PEG-LP mostly directed to tumor cells due to extravasation as well as it partly targeted the TECs (yellow dots). Very few amount of large size PEG-LP was detected in the tumor, indicating its capability to minimize the EPR effect. Large size RGD-PEG-LP was found mostly within the tumor vessels indicated that it preferentially targeted the TECs. Scale bars 50 μm.

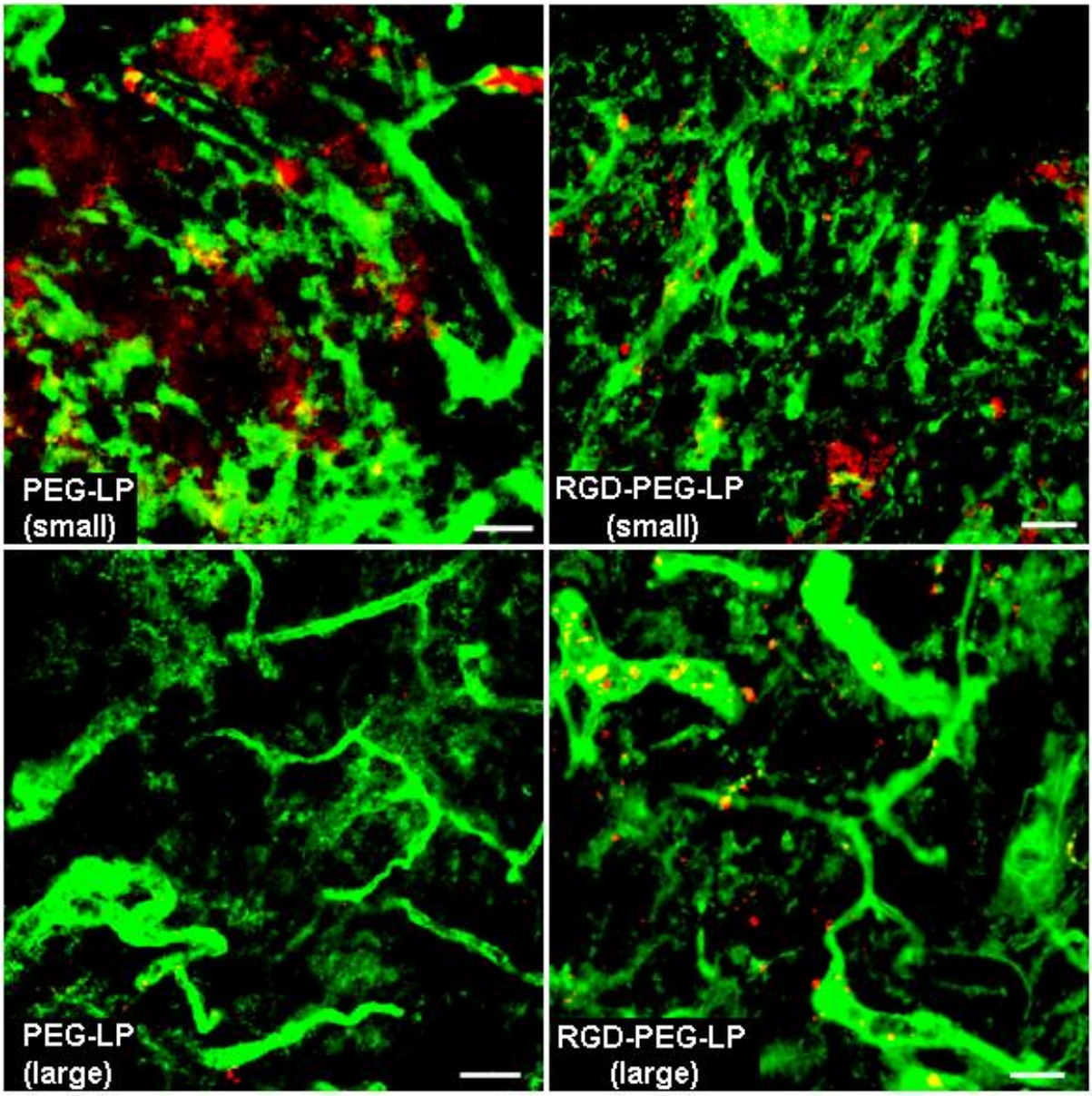


Fig. S3. In vitro delivery of DOX to HUVEC by different size PEG-LPs. HUVEC cells were incubated with 10 μg/ml of DOX (as free drug or encapsulated within the PEG-LPs) for 30 min at 37 °C, followed by observation under CLSM. Blue: DAPI, red: DOX, scale bars 20 μm.

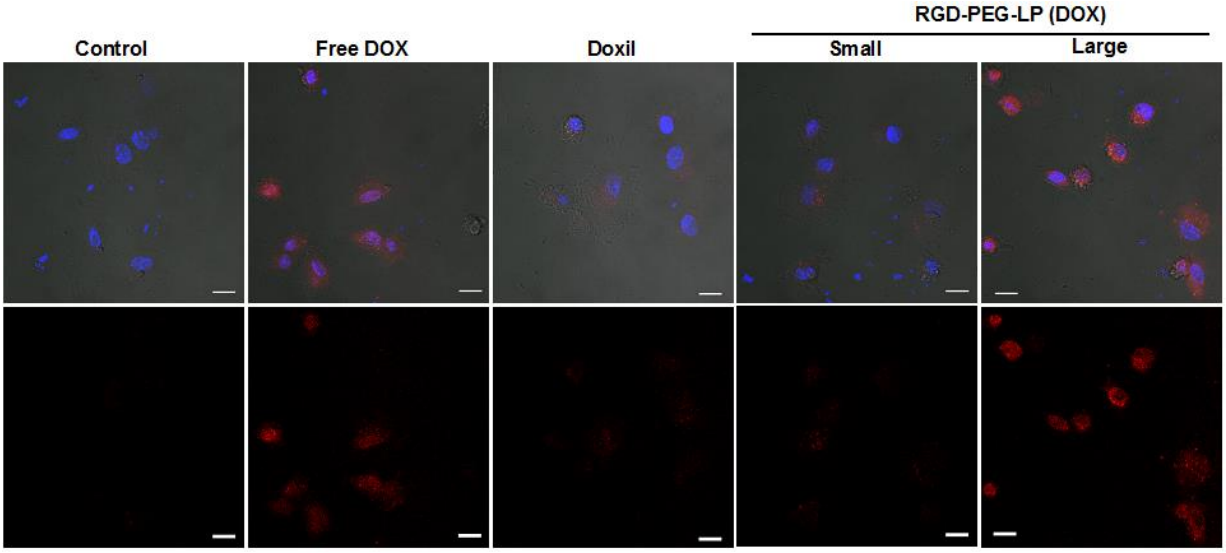


Fig. S4. Observation of the rate of growth of OSRC-2 and OSRC-EC. Five thousand cells were plated in 96-well plate and incubated for 24 h at 37 °C. The cells were washed with PBS and re-incubated with a cell counting kit-8 (CCK-8) solution for 2 h and absorbance was measured at 450 nm using a microplate reader (Thermo Fisher Scientific Inc.). The tetrazolium salt, present in the CCK-8, is reduced by dehydrogenase activities in cells to give a yellow-color formazan dye and the amount of the generated dye is directly proportional to the number of living cells. No significant difference in fluorescence intensities was observed, indicating the similar growth rate of OSRC-2 and OSRC-EC cells. Data are presented as mean±SD (n=5). Statistical analysis was performed by the two-tail unpaired t-test. N.S, not significant.

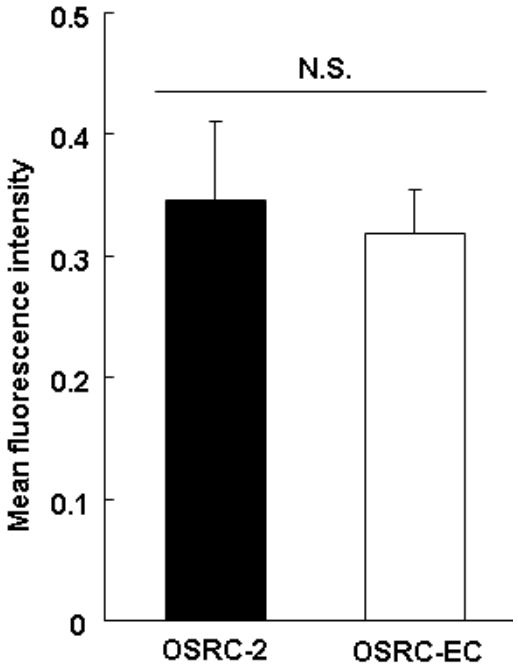


Fig. S5. Schematic representation of the site of action of different size PEG-LPs in tumor tissue. Small size PEG-LPs having ~100 nm in diameter (nm in diameter, dnm) generally accumulate in tumor tissue via the EPR effect through the leaky tumor vasculature. It is possible that large size PEG-LPs (~300 dnm) minimize the EPR effect. Modification of large size PEG-LP with specific ligand (RGD) would lead the higher interaction with the target receptor (Integrin $\alpha v\beta 3$) present on the surface of tumor endothelial cells (TECs); consequently, provide its cytotoxic effect on TECs, this then leads death or suppression of the growth of tumor cells in a blood supply manner (anti-tumor effect).

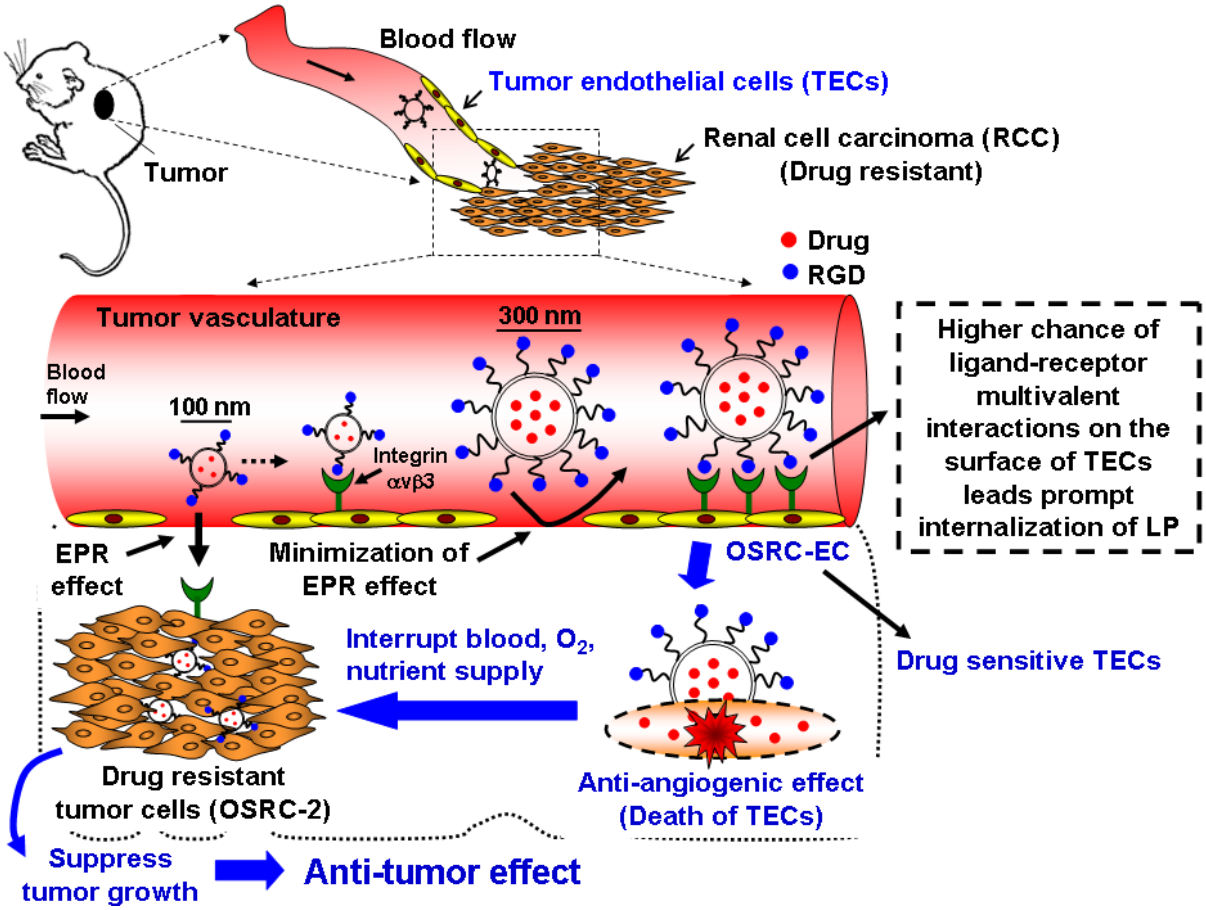


Fig. S6. Observation of cell apoptosis in normal organs.

OSRC-2 tumor bearing mice (n=4) were treated with three successive once daily dose of 1.5 mg/kg doxorubicin in PEG-LPs or were untreated with PBS (control). Liver, spleen, lung were excised at 24 h of post injection. Images of the organs were obtained by confocal microscopy. The area of the green signals derived from the apoptotic cells in normal organs was counted from at least 20 images taken from different positions in the organs. Statistical analysis vs control was performed by one-way ANOVA followed by Dunnett-test. *P<0.05; **P<0.01; N.S, not significant.

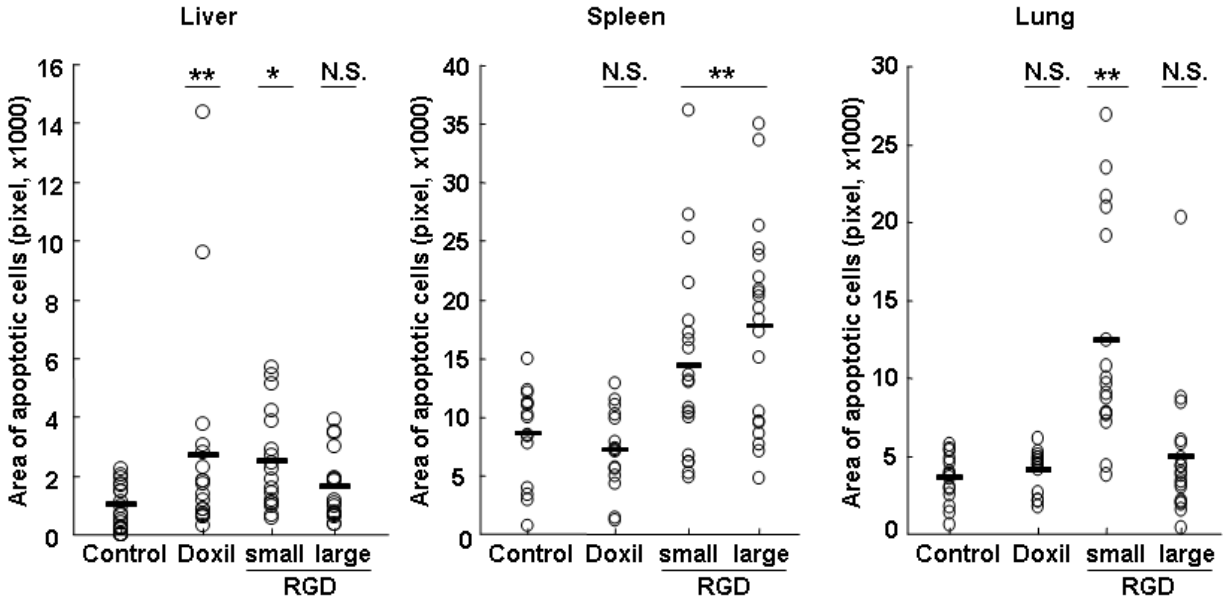
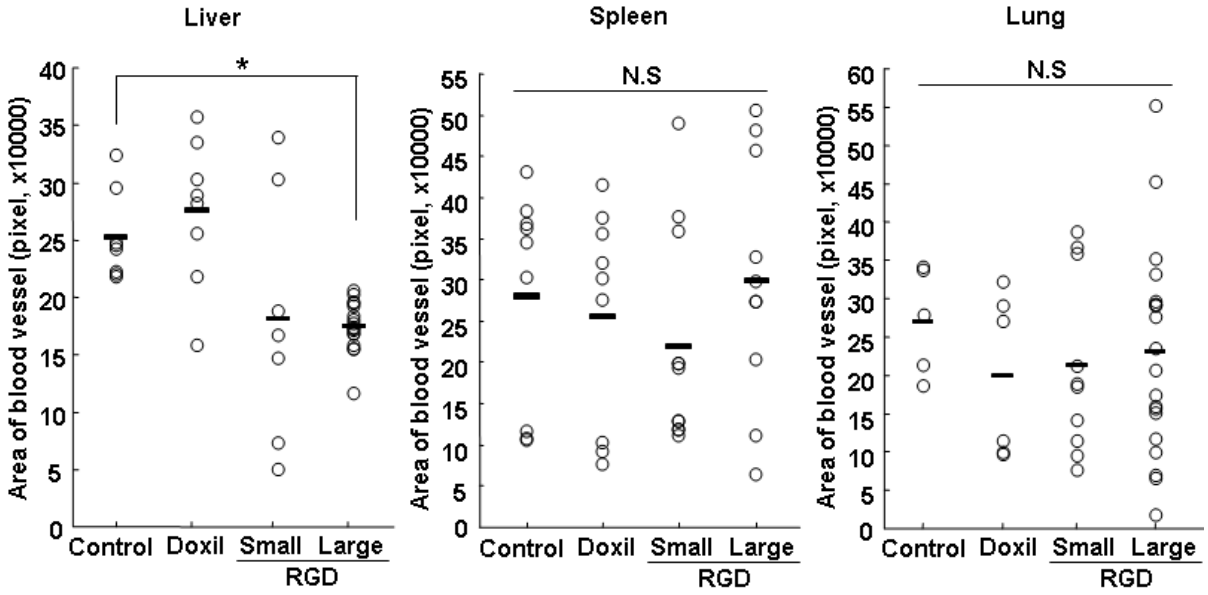


Fig. S7. Quantitative analysis of the density of the normal blood vessels treated with PEG-LPs (DOX). Mice bearing OSRC-2 tumor were treated with PBS (control) or three successive once daily dose of 1.5 mg/kg doxorubicin (i.v. injection via tail vein) in PEG-LPs. At 24 h post-injection, the animals were sacrificed; organs were collected and stained with FITC-Isolectin (for blood vessel) and Hoechst 33342 (for nuclei) followed by analysis under CLSM. After taking the images from three independently studied mice for each PEG-LP (DOX), the area of blood vessels was counted from at least 10-20 images taken from different positions in the organs. Scale bars 50 μm. Statistical analysis vs control was performed by Bonferroni One-way ANOVA followed by Dunnett-test. *P<0.05; N.S, not significant.



Supplementary Tables

Table S1. Physical properties of DOX loaded PEG-LPs prepared using HSPC, Cholesterol as lipid components.

Sample ID		Diameter (nm)	PDI	Zeta-potential (mV)
Small size	Doxil	103±8	0.13±0.02	-12±3
	RGD-PEG-LP	114±8	0.12±0.02	-14±4
Large size	PEG-LP	326±38	0.17±0.04	-8±3
	RGD-PEG-LP	331±42	0.18±0.04	-12±4

The data are expressed as the mean±SD value from at least six different preparations.

Table S2. Therapeutic efficacy of various formulations of DOX loaded PEG-LPs in OSRC-2 tumor-bearing BALB/c mice.

Treatment group	Tumor growth rate (mm^3/day)	T/C (%)	MST	ILS (%)
Control	399.45	-	17±6	-
Doxil	334.55	83.75	22±12	33
RGD-PEG-LP (small size)	339.24	84.93	26 ±10	57
RGD-PEG-LP (large size)	203.51	50.95	29±11	73

Results are expressed as the mean±SD (n =5). The T/C index was obtained by dividing the growth rate in the treatment group (T) by that in the PBS-treated group (C). MST denotes mean survival time, ILS denotes increased life span.